University of Alberta

Fabrication, Modeling and Experimental Study of Bending Deformation of Micro-Ferrogel Fibers in a Non-uniform Magnetic Field

by

Tasnuva Khaleque

A thesis submitted to the Faculty of Graduate Studies and Research in partial fulfillment of the requirements for the degree of

Master of Science

Department of Mechanical Engineering

Fall 2009
Edmonton, Alberta

Examining Committee

Dr. Walied Moussa (Supervisor), Department of Mechanical Engineering

Dr. Yongsheng Ma, Department of Mechanical Engineering

Dr. Samer Adeeb, Department of Civil and Environmental Engineering

To my parents

Abstract

Hydrogel smart polymers have achieved a great attention in the research area of drug delivery, MEMS/NEMS, microfluidics and sensor design because of their responsiveness to various environmental stimuli- pH, temperature, light, electric field, enzyme etc. This thesis presents the modeling, fabrication and study of the bending deformation of magnetic field sensitive hydrogel micro fibers called ferrogels. The objective is to externally actuate the ferrogel fibers by applying magnetic field, for the application of targeted drug delivery inside the alveoli of a human lung. Prediction of the bending deformation of the ferrogel fibers is done by the Multiphysics Finite Element Modeling in an Arbitrary Lagrangian Eulerian (ALE) framework. Ferrogel micro fibers are fabricated and the bending deformation is studied experimentally by varying the aspect ratio of the fibers, volume fraction of the magnetic particle content of the fibers and the magnetic field strength. The numerical and experimental results are compared. This is the first attempt to numerically predict the bending deformation of ferrogel micro-fibers.

Acknowledgements

I would like to use this opportunity to express my sincerest thanks to my supervisors Dr. Walied Moussa and Dr. Warren Finlay for their continuous guidance, encouragement, financial support and advice on my academic works and life at the University of Alberta. I am delighted to have this opportunity to involve in this fascinating project and friendly research group.

I am especially thankful to Dr. Sami Abu Salih for the time and effort he had put into my research work while working as a post doctoral fellow in the Advanced MEMS/ NEMS Multiphysics Design Lab. Thanks also to all present and past members of my research group for providing a good working atmosphere.

Lastly I would like to acknowledge the support from my friends and family. I want to express deep gratitude to my parents for their love and endless support. I also like to thank my husband, my three sisters, and family for their love and support.

Edmonton Alberta — Tasnuva Khaleque

September, 2009

Table of Contents

Chapter 1 Overview 1

Chapter 2 Theory and Background 4

2.1 Drug Delivery 4

2.2 Micro Fibers 7

2.3 Actuation 8

2.4 Smart Polymer Hydrogel 10

2.4.1 Composition of Hydrogel 10

2.4.2 Hydrogel Fabrication 11

2.4.3 Actuation of Hydrogel 13

2.4.3.1 pH Actuation 14

2.4.3.2 Electric Field Actuation 15

2.4.3.3 Temperature Actuation 15

2.4.3.4 Ultraviolet and Visible Light Actuation 17

2.4.3.5 Magnetic Field Actuation 17

2.4.3.5.1 Magnetic hydrogel/Ferrogel 18

2.4.3.5.2 Background Study of Ferrogel 18

2.5 Basic Magnetism 23

2.5.1 Basic Magnetic Terminology 23

2.5.2 Classification of Magnetism and Magnetic Materials 25

2.5.2.1 Diamagnetism and Diamagnetic Material 26

2.5.2.2 Paramagnetism and Paramagnetic Material 26

2.5.2.3 Ferromagnetism and Ferromagnetic Material 27

2.5.3 Ferrofluid 28

Chapter 3 Multiphysics Modeling of Ferrogel Fiber 33

3.1 Modeling Approach 33
3.1.1 Maxwell's Equations 34
3.1.2 Arbitrary Lagrangian-Eulerian (ALE) Methods 35
3.2 Model Overview 36
3.2.1 Material Properties 39
3.2.2 Boundary Conditions 42
3.2.3 Mesh Generation 42
3.3 Verification of the Model 43
3.4 FEM Results 45
3.4.1 Straight Fiber Models 45
3.4.2 Stepped Fiber Models 47
Chapter 4 Fabrication of Ferrogel Fibers and Experiments 64
4.1 Fabrication of Ferrogel Fiber 64
4.1.1 Fabrication of Silicon Master and PDMS Micro Beakers 65
4.1.1.1 Design 65
4.1.1.2. Photomask Generation 66
4.1.1.3. Silicon Master by Etching 67
4.1.1.3.1 Cleaning 67
4.1.1.3.2 Thermal (Silicon dioxide) Layer Growth 67
4.1.1.3.3 Spin Coating Resist and Soft Bake 68
4.1.1.3.4 Exposure and Development 69
4.1.1.3.5 RIE (Reactive ion etching) 70
4.1.1.3.6 Dry Etch - BOSCH® Process 71
4.1.1.4 Silicon Master Fabrication by SU-8 process 72
4.1.1.4.1 Dehydration Bake 72
4.1.1.5 Spin Coating and Soft Baking 72
4.1.1.5.1 Lithography 73

4.1.1.5.2 Post Exposure Bake 74
4.1.1.5.3 Developing 74
4.1.1.6 Cast Molding 74
4.1.1.7 Ferrogel Fabrication Procedure 76
4.2 Experiment 78
4.2.1 Experimental Setup and Procedure 78
4.2.2 Results and Discussions 79
Chapter 5 Conclusion and Future Work 90
Bibliography 91
Appendix A 98
A.1 Magnetic Dipoles 98
A.2 Magnetic Dipole Interaction in External Fields 98
A.3 Force on a Magnetic Dipole in a Non-uniform Filed.................................... 100
Appendix B 102

List of Figures

2-1 Structure of anionic hydrogel……………………………………………………29

2-2 Structure of cationic hydrogel…………………………………………………...29

2-3 Swelling mechanism of Hydrogel by pH stimulation……………………………...30

2-4 (A) Elongation of ferrogel……………………………………………………….31

(B) Contraction of ferrogel………………………………………………………...31

(C) Bending of ferrogel…………………………………………………………….31

2-5 B-H plot of ferromagnetic material………………………………………………...32

3-1 (a) Lagrangian description of particle motion……………………………………...48

(b) Eulerian description of particle motion………………………………………...48

(c) ALE description of particle motion……………………………………….....48

3-2 (a) A straight ferrogel fiber of length L and cross section axa……………………49

(b) 2-D view of a straight ferrogel fiber……………………………………………49

3-3 Model set-up of the numerical investigation of micro-ferrogel fiber……………..50

3-4 Flow chart of the Multiphysics modeling technique of ferrogel fiber…………….51

3-5 Steps of making stepped ferrogel fibres from a straight fibre ……..……………...52

3-6 The numerical model set-up with appropriate boundary conditions……………...53

3-7 The straight ferrogel fibre model with mesh (AR-40)…………………………….54

3-8 Mesh sensitivity test, maximum deformation, d, mm vs. number of elements…...55

3-9 Stepped fibre model with mesh……………………………………………………56

3-10 The magnetic field strength, B [T] vs. distance z, mm plot for Zrinyi *et al* experiment and the experimental set-up [6]…………………………………………….57

3-11 Deformation vs. current intensity of present numerical analysis and the experimental results of Zrinyi *et al.*[6]…………………………………………………………...58

3-12 Maximum deformation of straight ferrogel fibres vs. volume fraction of magnetic particles for Aspect Ratios 40, 35, 30, 25, 20, 15 and 10. A, B and C are constants…... 59

3-13 Maximum deformations vs. aspect ratio plot for different volume fraction of magnetic particle content of the fibres. A, B and C are constants.…………..………....60

3-14 Maximum deformations vs. magnetic field strength (AR 40, 1% volume ratio). A and B are constants……………………………………………………………………...61

3-15 comparison of maximum deformation of ferrogel fibers (straight) between the model with and without ALE framework……………………………………………..62

3-16: comparison of maximum deformation between stepped and straight ferrogel fibres ……………………………………………………………………………………….....63

4-1 Steps of fabricating silicon master……………………………………………..82

4-2 Steps of fabricating PDMS micro-beakers……………………………………...83

4-3 The arrangement of the mask-aligner and the photomask used to polymerize the ferrogel precursor……………………………………………………………………...84

4-4 (a) The Experimental Setup……………………………………………………85

(b) The microscope equipped with the camera…………………………………...86

4-5 The method of measuring the bending deformation of the ferrogel fiber………..87

4-6 Comparison between Experimental and Simulation deformation of the ferrogel fibers…………………………………………………………………………………..89

4-7 Comparison between numerical and experimental results for the maximum deformation due to the variation of magnetic field strength (AR 40, 1% VR)…………..90

List of symbols

χ	magnetic susceptibility
μ_0	magnetic permeability in the vacuum, H/m
μ_r	relative magnetic permeability
B	magnetic flux density, mT
H	magnetic field strength
M	magnetization
L	length of the ferrogel fiber, mm
a	width of the fiber, mm
n	number of ferromagnetic particle
k_B	Boltzmann Constant
T	temperature
m	magnetic moment of individual magnetic particle of ferrofluid
v, φ_m	volume fraction of magnetic particle in ferrogel
$M_{s,f}$	saturation magnetization of individual magnetic particle
R	radius of magnetic particle
AR	aspect ratio of the fiber

CHAPTER 1

OVERVIEW

In recent years, research involving hydrogel smart polymers are very popular. As a stimuli responsive material, hydrogels have attracted a great deal of interest due to their suitability in the application of controlled and targeted drug delivery [1], microfluidics [2], biomechanics [3], sensor design [4] and micro and nano-electromechanical systems (MEMS/NEMS) [5].

In this thesis the application of hydrogel in the targeted drug delivery is focused. Many researchers have studied hydrogels for application in the controlled and targeted drug delivery. The responsiveness of hydrogels to different stimuli such as temperature, pH, light, electric field etc. made them suitable for controlled and targeted drug delivery. Suitability of each of type hydrogel in the drug delivery application is studied by many researchers. The objective of this thesis is to fabricate magnetic field sensitive hydrogel fiber for the application in targeted drug delivery systems. The magnetic hydrogel fibers are studied experimentally and numerically in the present thesis.

Numerous works have been done on magnetic field sensitive hydrogels to use them as microactuators [6-14]. But their application in targeted and controlled drug delivery is limited and under investigation. No numerical work was done before on magnetic field sensitive hydrogels.

In Chapter 2, an overview of the controlled and targeted drug delivery is presented. A brief discussion on micro fibers and their application is presented in the second section. The third section of the chapter contains an overview of actuation. Then an introduction to the smart polymer hydrogel, its different stimulation methods, and its fabrication is included. A detailed background study of the magnetic field sensitive hydrogel is presented in this chapter 2. The basic theory of magnetism is briefly described at the end of the chapter.

In Chapter 3, introduction to Maxwell's equations and Arbitrary Lagrangian Eulerian (ALE) method are presented. The development of finite element model of magnetic field sensitive hydrogel fibers is discussed throughout the chapter. The model consists of Maxwell's equations and the simulation was done in the ALE framework. Validation of the model was also included in chapter 3.

In chapter 4, the detailed fabrication technique of the magnetic hydrogel fibers and the problems encountered during the fabrication process are presented. The experiments involving the magnetic hydrogel fibers are then discussed in detail. A comparison between numerical and experimental results is also presented in Chapter 4.

In chapter 5, a brief conclusion is presented from this present thesis and possible further extension is recommended.

CHAPTER 2

THEORY AND BACKGROUND

The main objective of this thesis is to externally actuate magnetic field sensitive smart polymer hydrogel fiber for the application of targeted drug delivery inside the alveoli of a human lung. In this chapter an overview of the controlled and targeted drug delivery is presented. A brief discussion on micro fibers and their application is presented in the second section. The third section contains an overview of actuation. Then an introduction to the smart polymer hydrogel, its different stimulation methods, and its fabrication is included. A detailed back-ground study of the magnetic field sensitive hydrogel is presented in this chapter. The basic theory of magnetism is briefly described at the end of the chapter.

2.1 Drug Delivery

Drug delivery is the process of delivering formulated drugs to the required site of action in the human body. The objective of a drug delivery system is to deliver drugs to the site of action at the proper rate and concentration to minimize side effects and maximize therapeutic effects [15]. Drug delivery systems can be divided into two broad categories- 1.Controlled drug delivery 2.Targeted drug delivery.

Controlled drug delivery is the process of releasing a drug at a predetermined rate. In a controlled drug delivery system, the site of drug release and the site of action are different. Drug is released in a systematic circulation. This is done to allow the drug to take more time to reach the desired site and thus allow the effective therapeutic dose at the desired site. Also to reduce the side effects of excessive dose that exceeds the therapeutic amount [16].

Targeted drug delivery is the process of releasing a drug at or near the site of action. The main objective of targeted delivery is to get high local drug concentration at the site of action [16]. Physical controls such as localized magnetic fields, pH differences, temperature gradients etc. can be used to direct the drug to the specific site of action.

In controlled drug delivery, to achieve the desired concentration of the drug at the site of action, a higher concentration is delivered to the body, and before achieving the correct concentration at the site of action a great amount is wasted in the normal tissues which may cause many negative side effects [17]. The advantage of targeted drug delivery over controlled drug delivery is that, in targeted drug delivery the drug is administered only at the site of action thus reducing the possibility of negative side effects of controlled drug delivery. In the case of lung disease, the drug is delivered to the alveoli by targeted drug delivery. This thesis focused on the targeted drug delivery to the human alveoli by magnetically actuated smart polymer hydrogel fiber.

Liposomes, antibodies, polymers, etc. are used as drug carriers. Polymers having biocompatibility and biodegradability properties are suitable for both controlled and targeted drug delivery systems. Both natural and synthetic polymers are suitable for drug carriers as they have little or no toxicity [16]. They are easy to process, and their physical and chemical properties can be controlled through molecular synthesis [18]. Polymers have many more advantages as drug carriers over liposomes and antibodies [19].

It is found that constant concentration of a drug is not always the best treatment [16] . Sometimes it is necessary to maintain the nonlinear release of drugs. Also sometimes it is important to dictate to the carriers where to deliver the drug (in case of targeted drug delivery) and with which time interval. External stimuli responsive carriers can serve these purposes. Temperature, pH, visible lights, electric fields, magnetic fields etc are some external stimuli that are used to change the rate of drug release [16]. Hydrogels are environmental sensitive smart polymers suitable to use as drug carriers. They are sensitive to temperature, pH, visible and ultraviolet lights, electric fields, enzyme, etc. They are extensively used in controlled drug release, because of their responsiveness to external stimuli. Their availability, ease of fabrication, biocompatibility and biodegradability also make them suitable to use as drug carriers [20, 21]. In this thesis magnetic field sensitive hydrogels are fabricated for use in the targeted drug delivery to a human lung. Hydrogels can be fabricated in numerous shapes and they can be actuated by the external stimuli to which they are responsive. Later in this chapter the various actuation methods of hydrogels are explained and the best actuation method for targeting drug to the alveoli is found to be magnetic actuation.

2.2 Micro Fibers

Fibers are a group of materials which are continuous elongated filaments that can be spun into yarn. The word fiber illustrates an object that has high aspect ratio with axisymmetric or near axisymmetric cross-section.

Fibers are of two types: natural and synthetic (man made). Natural fibers are made from plants, animals and mineral sources. They are mainly composed of cellulose and protein, while synthetic fibers are usually made of nylon, polyesters, acrylic and polyethylene etc. Depending on the source natural fibers can be classified as vegetable fibers and animal fibers. Natural fibers are biodegradable over time.

We ingest natural fibers everyday with our foods. Some food fibers are soluble while others are insoluble. Soluble fiber dissolves in water and helps the digestive process, lower total cholesterol therefore reducing the risk of heart disease; regulate blood sugar for people with diabetes. They are found from oat products, beans and nuts, fruits such as oranges and apples and vegetables such as carrots. Insoluble fiber, found in whole-wheat products, green leafy vegetables etc. promotes regular bowel movement, removes toxic waste through colon in less time and prevents colon cancer.

Synthetic fibers have superior strength and dimensional integrity. The subsets of synthetic fiber are mineral and polymer. They have diverse applications such as in textile industries, filtration, drug delivery, tissue engineering etc.

In this thesis, actuation of magnetic field sensitive hydrogel fiber, which is synthetic in nature, is studied for targeting the drug to the human alveoli. Actuation of a fiber means enforcing the deformation of the fiber such as bending, elongation or contraction. Bending of hydrogel fiber is investigated in this thesis. Bending of the fiber beyond the mechanical strength can cause the fiber to crack and release the drug in the targeted site of action.

2.3 Actuation

Actuation is the act of putting something into motion. Some microelectromechanical system (MEMS) devices have moveable parts to act as microactuators. For moving a stationary object mechanical energy is needed. This mechanical energy can come from an electric field, temperature change, pH difference, chemical reaction, light, magnetic field etc.

All solid materials expand with increase in temperature and shrink when the temperature is decreased. Using this principle it is possible to generate displacement in MEMS devices. Microactuators that work on this principle are known as thermal actuators.

A charged particle creates an electric field around it. All the charged particles experience force in an electric field. Electrostatic actuators work on this principle. In a uniform magnetic field the magnetic particles experience no net force. The magnetic force is generated by a non-uniformly distributed magnetic field according to the following equation

$$F = \frac{1}{2\mu_0} \Delta\chi V \nabla \mathrm{B}^2 \tag{2.1}$$

Where $\Delta\chi$ is the difference in the magnetic susceptibility between the particles and the medium, V is the volume of the particle and B is the B-field. A detailed derivation of equation (2.1) can be found in Appendix (A). From this equation it is found that magnetic force is proportional to the difference in magnetic susceptibility, volume, and the magnetic flux density field gradient. When suspended in a weakly magnetic medium, such as water, a piece of paramagnetic or ferromagnetic material will experience force in the direction of the gradient of the magnetic flux density field. A diamagnetic material in the same medium will experience force in the opposite direction. In other words, paramagnetic or ferromagnetic materials will be attracted toward the maxima of the magnetic flux density field, while diamagnetic materials will be attracted toward the minima of the magnetic flux density field. Magnetic actuators work on this principle.

2.4 Smart Polymer Hydrogel

Hydrogels are three dimensional cross-linked polymer networks. They are considered as smart materials, as their responsiveness to different environmental stimuli made them popular in the research area of MEMS/NEMS, drug delivery, biomechanics etc. the composition of hydrogel, its fabrication methods and stimulation techniques are included in sections 2.4.1, 2.4.2 and 2.4.3 respectively.

2.4.1 Composition of Hydrogel

The polymer chains of hydrogels are interconnected through crosslinks and are immersed in aqueous solution [22, 23]. The polymer network may be hydrophilic and/or hydrophobic [24]. The hydrophilic components cause the hydrogel to swell, whereas the hydrophobic components control the swelling of the gel as well as the mechanical properties [25]. There are generally ionizable basic or acidic groups attached to these polymer chains, with some of these ionizable groups dissociating completely and others dissociating partially in solutions [22, 26]. Anionic hydrogels have negative ions which are bound to the polymer network, shown in Figure 2-1, while cationic hydrogels have fixed positive ions, seen in Figure 2-2, and neutral hydrogels contain the same amount of both positive and negative fixed ions. It is generally assumed that neutral hydrogels have a nearly identical concentration distribution of fixed ions throughout the polymer matrix. Hydrogels are considered super absorbent because they can absorb large amounts of surrounding water or solvent. The amount of water absorbed by the hydrogel depends on the balance between the stimuli induced osmotic pressure and the inherit elastic restoring force of the polymer network. For large value of elastic restoring force the gel absorbs, comparatively, less water than for lower values.

The composition of hydrogels varies with the polymerization monomer composition that are used to fabricate hydrogels [27]. The most general structure of hydrogel consists of backbone monomer, crosslinking co-monomer, electrolyte co-monomer, and solvent [28].

Based on the types of bonding that exists between the polymer chains, hydrogels can be classified as physical gels or chemical gels. In physical gels the polymer chains are held together via polymer chain entanglement or non-covalent bond with the attractive forces induced by the hydrogen bonding or hydrophobic forces. In chemical gels the polymer chains are bound to each other by covalent bonds [27].

2.4.2 Hydrogel Fabrication

Hydrogels can be fabricated by a number of different techniques. Two methods are most common 1.photopolymerization with photoinitiator: copolymerization and crosslinking of co-monomers by using cross-linking agents where the polymerization reaction is initiated by photoinitiator [29] 2. Photoinitiator free photopolymerization: linear polymer can be crosslinked using chemical compound or irradiation in the absence of any crosslinking agent and initiator [29, 30].

In the first method, co-monomers, crosslinking agent and photoinitiator are mixed and are exposed to the ultraviolet light through a photomask. The photoinitiator upon irradiation absorbs light and creates free radical to initiate polymerization and forms crosslinked hydrogel. The hydrogels fabricated then washed/flushed with distilled water to remove the unpolymerized liquid mixture [29, 31].

In the second method, gamma and electron beam radiation are used to prepare hydrogels. The irradiation of linear polymer chains forms radicals on the polymer chains. Also this irradiation forms hydroxyl radicals from water molecules and these two types of radicals combine together and form covalent bond between polymer chains. As a result a crosslinked structure is formed [29, 30, 32].

Both pH and temperature sensitive hydrogels can be fabricated using the first method, using methaycrylic acid and isopropylacrylamide monomers, respectively. Polymerization of pH sensitive hydrogels can also be achieved using gamma-irradiation [30, 32], hydrodynamic fabrication via ultra-violet light [33, 34], heat induced esterification [35], and free radical polymerization [36]. Fabrication of electrically-stimulated hydrogels can be performed using the aforementioned processes for pH sensitive hydrogels, since electrically-stimulated hydrogels are compositionally the same as pH sensitive hydrogels.

Multiple methods exist to fabricate hydrogels sensitive to thermal stimulation. Some of the main fabrication methods include, UV-photolithography [37], e-beam and gamma-ray irradiation [38], free-radical cross-linking copolymerization [39], a hybrid technique combining free-radical copolymerization and freezing polymerization [40]. In addition, some techniques fabricate with sodium carbonate [41] or dodecyl dimethyl benzyl ammonium bromide (DDBAB) [42] to generate a highly porous structures.

2.4.3 Actuation of Hydrogel

Hydrogels are responsive to a wide range of external stimuli such as pH [43], temperature [44], solvent [45], electric field [46], visible and ultraviolet lights [47], enzymes [48] etc. With a small change in these environmental stimuli hydrogels swell or deswell. The swelling-deswelling capability of intelligent polyelectrolyte hydrogels has received increased interest from researchers in micro and nano electromechanical systems (MEMS/NEMS), microfluidics [2, 5], drug/controlled delivery systems [1], biomechanics [3], and sensor design [4]. This section reviews the stimulation methods of pH, electric field, temperature, visible and ultraviolet light, magnetic field and their associated mechanism for volume transition.

2.4.3.1 pH Actuation

The swelling and deswelling of hydrogels due to a pH change is reversible and repeatable [2, 43, 49, 50]. pH sensitive hydrogels have either acidic and/or basic groups bound to their polymer chains, referred to herein as cationic and anionic hydrogels, respectively. At high pH the acidic groups of anionic hydrogels deprotonate and at low pH the basic groups protonate [2, 51]. As the pH of the surrounding solvent changes, an ion concentration gradient is established between the inside and outside of the gel. This gradient causes diffusion of mobile ions into and out of the hydrogel, and most importantly causes an osmotic pressure to be established on the surface of the hydrogel. This osmotic pressure, expanding or compressing the hydrogel, causes the desired volume transition. The diffusion of ions, from solvent into the hydrogel also results in imbibes of solvent inside the hydrogel. Anionic hydrogels swell at high pH, with the ionic composition depicted in Figure 2-3, while cationic hydrogels swell at low pH [43, 52]. Swelling of the hydrogel induces elastic restoring forces within the polymer network, which balances the osmotic pressure, resulting in an equilibrium gel state. The degree of swelling/deswelling within a hydrogel depends on the osmotic pressure generated, induced by the concentration gradient of mobile ions, and the elastic restoring force. This restoring elastic force plays a significant role for balancing the osmotic pressure in order to get the hydrogel in a equilibrium state [22, 26].

In this thesis, the objective is to externally actuate hydrogel fiber for targeting drug delivery to human lung. pH actuation is not possible in this case.

2.4.3.2 Electric Field Actuation

Hydrogels swell, shrink, and bend in response to electrical stimulus using a very similar mechanism as that described for pH stimulus. The major difference, and advantage, between pH and electrical stimulation is that the ions are forced to set-up a gradient through the application of an electrical field [46, 53-55]. This electric field forces ionic migration instead of allowing the much slower diffusion based processes to establish ionic gradients. The ionic gradients established can be much larger than that provided by pH stimulation [56], which causes a larger osmotic pressure to be established resulting in faster response times [53]. In addition, reversing the polarity of the electric field reverses the concentration gradients, and subsequently causes the osmotic pressures previously established to act in the opposite direction. This easy and fast switching of a hydrogels volume transition can be exploited for increased microvalve response and micropump design.

As the electrical resistivity of human tissues is very high, external electric field actuation of the hydrogel fiber is not possible.

2.4.3.3 Temperature Actuation

Temperature sensitive hydrogels contain both hydrophobic and hydrophilic groups bound to their network. They undergo volume changes (swelling/deswelling) either at lower critical solution temperature (LCST) or upper critical solution temperature (UCST) [20, 50, 57, 58]. Temperature sensitive hydrogels are classified as negatively temperature sensitive, positively temperature sensitive and thermally reversible hydrogels [20, 50, 58]. Negatively temperature sensitive hydrogels deswell as the temperature of there buffer increases above the LCST. On the other hand, positively temperature sensitive hydrogels deswell as the temperature decreases below the UCST [20, 50, 58, 59]. The degree of temperature sensitivity of hydrogels depends on the temperature dependency of the hydrogen bonding and hydrophobic interactions. In case of low temperature of negatively temperature sensitive hydrogels, the hydrogen bonding of water molecules is strong near the hydrophobic polymer chains. This lowers the mixing free energy and increases the solubility of polymer chains in water and as a result the hydrogel swells. But at high temperature the hydrogen bond becomes weak and the hydrophobic interaction is dominant and the gel shrinks [43, 60, 61]. Also as the temperature increases the hydrophilic/hydrophobic balance of the polymer network is disturbed, leading to dehydration and the gel shrinks [59].

Temperature sensitive hydrogels are not biocompatible [21]. The monomers and crosslinkers used to fabricate temperature sensitive hydrogels are found to be toxic. Also some temperature sensitive hydrogels are not biodegradable. As the aim of the current thesis is to use hydrogel as drug carrier to the human lung, temperature sensitive hydrogels can not be used.

2.4.3.4 Ultraviolet and Visible Light Actuation

Light sensitive hydrogels are classified as UV light sensitive and visible light sensitive hydrogels [58, 62]. Some UV light sensitive hydrogels contain a UV light ionizable molecule, leuco cyanide [58, 62, 63]. Upon irradiation of UV light the leuco cyanide ionized and cyanide ions cause an increase in osmotic pressure and the gel swells. Visible light sensitive hydrogels contain chromophore, and when exposed to visible light the chromophore absorbs light and then dissipates as heat. As a result the temperature of the gel increases which results deswelling of the gel similar to the temperature sensitive hydrogels [62, 64, 65].

Light can not pass through human body. So, external actuation of hydrogel fiber using light is not possible.

2.4.3.5 Magnetic Field Actuation

Magnetic permeabilities of human tissues are equal to that of free space; as a result magnetic field wave can pass easily through human tissues [66]. So to externally actuate a hydrogel fiber inside human lung, magnetic field actuation is the best choice.

An introduction to magnetic field sensitive hydrogels (ferrogels) and detailed background study are presented in the sections 2.4.3.5.1 and 2.4.3.5.2 respectively.

2.4.3.5.1 Magnetic hydrogel/Ferrogel

Magnetic filed sensitive hydorgel, also called a ferrogel, is also a stimuli responsive hydrogel. Ferrogels are three dimensional crosslinked polymer networks those are swollen by ferrofluids and are thus sensitive to magnetic field. They are loaded with a special type of strong magnetic (ferromagnetic) filler particles [6, 7, 10]. In ferrogels fine ferromagnetic nanoparticles are embedded into the flexible polymer networks and thus exhibits magnetoelastic behavior [6, 7, 9, 67]. With the application of magnetic field these gels show abrupt shape changes such as elongation, contraction, bending etc. This shape change capability makes ferrogels a new promising material in the group of stimuli responsive gels. They are often used as soft actuators (artificial muscles) [10, 13], controlled drug delivery [68], hyperthermia treatment [69] etc.

2.4.3.5.2 Background Study of Ferrogel

Many researchers have devoted their efforts to the development of magnetic field sensitive hydrogels/ferrogels. For example Zrinyi *et al.,* Szabo *et al.* and Barsi *et al.* [6, 7, 9-13, 67, 70-74] fabricated hydrogels by mixing ferrofluids with chemically crosslinked poly (vinyl alcohol) hydrogels. The ferrofluid introduces monodomain, magnetite particles of colloidal size into poly (vinyl alcohol) hydrogels. The fabrication flow chart of the ferrogel by Zrinyi *et al.* is given in Appendix B. Depending on the fact that ferrogel experiences no net force in a uniform field; a shape change (elongation, contraction and bending) of the gel was achieved by applying non-uniform magnetic field. In the applied magnetic field the magnetic particles attached to the gel network are attracted by the field and the whole gel-magnetic particle system move together towards the field. In the experimental set up of Zrinyi *et al.,* ferrogel tubes are hanged by a rigid copper thread in water vertically between the plane-parallel poles of an electro-magnet. The current intensity of the electromagnet was varied but the voltage was kept constant.

Zrinyi *et al*.[7] Investigated the magneto-elastic behavior of cylindrical gel tubes. They focused mainly on the preparation of magnetic field sensitive polymer gels and reported three different shape changes-elongation, contraction and bending of the cylindrical gel tubes. The experimental set ups for obtaining elongation, contraction and bending are shown in fig 2-4. To achieve bending the average field gradient of the non-uniform magnetic field should be perpendicular to the cylindrical gel axis. And to get elongation and contraction the field gradient should be parallel to the gel axis. The only difference between contraction and elongation set-up is the position of the electromagnets along the length of the gel. They observed the dependence of ferrogel tube elongation on current intensity of electromagnets for two different magnetite content of the gel. Also they observed the effect of cross-linking density on the magneto-elastic behavior of the ferrogel. From the investigation they concluded that magnetic force is more profound in gels with weaker crosslinking density. The shape changes occur within hundredths of a second with the turning on and off of the magnetic field gradient.

Zrinyi *et al*. [6] then focused mainly on the elongation of the magnetic field sensitive cylindrical gel tubes of approximately 120 mm long and 10-20 mm of diameter in a non-uniform magnetic field. The non-uniform magnetic field was generated by solenoid based electromagnets. The nature of the magnetic field distribution depends on the geometry and quality of electromagnets [74]. The strength of the non-uniform magnetic field generated by the electromagnet was varied by changing the steady current intensity in the solenoid. For different current intensity, i.e. for different magnetic field gradient the elongation of the ferrogel tubes was observed. It was found that the ferrogel elongation mainly depends on the solenoid current intensity. Also small hysteresis occurs as the solenoid current is turned off. They observed the magnetic force- current intensity dependence. From the elongation-current intensity and force-current intensity data they obtained linear elongation- force dependence i.e. Hookean elastic behavior of the ferrogel tubes. The elongation of the gel tubes were recorded for different axial position and it was found that higher field gradient results in larger elongation.

Zrinyi *et al*.[8], [75] studied the magnetic properties of ferrogels. They obtained the magnetization of the ferrogels experimentally and plotted the experimental magnetization against the magnetic induction. Simple equipment was used to measure the magnetization of the ferrogel. No hysteresis loop was found as the ferrogels are superparamagnetic. They also observed the effect of magnetite concentration on the initial susceptibility of the ferrogels and found a linear relationship. They also compared the elastic and magneto elastic behavior of ferrogels experimentally. To compare the elastic and magneto elastic behavior of the ferrogels, stress-strain curve is plotted for two different loading conditions. Load was applied on the gel in the absence of external magnetic field, i.e. no magnetic force on the ferrogel. Then magnetic force was applied to deform the ferrogel, having no external load. From the stress-strain plot of the two types of deformation, it is found that there is no significant difference between these two types of deformation [75]. In both of the cases the stress-strain dependence is straight line, but there is a slight difference between the slopes of the two straight lines. This difference in slopes is due to the fact that the magnetic force deformation is non-homogeneous along the axis of the cylindrical gels, which was found experimentally. Noncontinous elongation and contraction of the ferrogel was observed with the change in current intensity [8, 10]. With the small increase in current density the elongation of the gel slightly increases and at a specific current intensity the elongation increases abruptly and that increase is comparatively large. With the further increase in current density the displacement increases slightly. Contraction of the gel takes place with the decrease in current intensity. Same as the elongation abrupt contraction takes place at a certain decrease in current intensity. The contraction does not follow the same path as the elongation that is hysteresis is observed in the magnetoelasticity of the ferrogel. But this irreversibility of the displacement of the ferrogel is not always observed. With the initial position of the gel with respect to the electromagnet this behavior varies. With decreasing the distance between the gel and the electromagnet both the noncontinous displacement and the hysteresis decrease and at a certain distance continuous shape transformation occurs as shown in fig. They also derived an expression for the unidirectional magneto elastic properties of the ferrogels [75] and explained a theoretical interpretation of noncontinous shape transition [8, 10].

Zrinyi *et al*.[10] also reported the theoretical aspect for the design of magnetic field sensitive polymeric gel actuators. As contraction of ferrogels can be achieved with the application of non-uniform magnetic field, muscular contraction is mimicked by magnetic gels [12, 13]. The effect of uniform magnetic field on magnetic field sensitive gel is also studied [12, 76]. When randomly distributed magnetic gel beads are kept in a uniform magnetic field there is no net magnetic force on the gel beads due to the lack of magnetic field gradient. But there are magnetic interactions between the gel beads as the magnetic field induces magnetic dipoles. The beads either attract or repel each other and form a pearl chain like structure. This formation has different technological implications.

Ramanujan *et al*. [14] prepared magnetic field sensitive hydrogel using polyvinyl alcohol (PVA) hydrogel and Fe_3O_4 powder that contains micron sized particles of Fe_3O_4 instead of using ferrofluids. This polyvinyl alcohol (PVA)-iron oxide composite has both the elastic properties of PVA and the magnetic properties of iron oxide particles. This combined property makes them useful to use as magnetic field sensitive actuator. Ramanujan *et al.* [14] studied the deflection of cylindrical ferrogels in the presence of static magnetic field (created by permanent magnet). The degree of deflection depends on the magnetic field strength and Fe_3O_4 content. For each magnetic particle concentration, there is a threshold value of the magnetic field strength where maximum deflection occurs. This property makes ferrogels to use as on-off type transducer. Ramanujan *et al.* [14] also reported that the magnetic particle content does not change the elastic properties of PVA gel.

2.5 Basic Magnetism

This section briefly discusses the basic magnetic terminology and constitutive relations of magnetism, the classification of magnetic materials and the main constituent of the ferrogel, ferrofluid.

2.5.1 Basic Magnetic Terminology

The response of any material to the applied magnetic field can be classified by some key magnetic properties of the material, the susceptibility, permeability, and coercivity. Magnetic field H can be thought of as the field created by the current flow in wires and the magnetic flux B as the total magnetic field that also contains the contribution of the magnetic properties of the materials in the field. The magnetic flux density (B-field) in free space under the applied magnetic field (H-field) can be expressed as

$$B = \mu_0 H \tag{2.2}$$

Where μ_0 is the magnetic permeability of free space, which is a fundamental physical constant and defines how much magnetic flux, can pass through space due to applied magnetic field. In SI unit the numerical value of μ_0 is 4Π×10e-7 H/m. When a piece of material is introduced into the applied field, the B-field is equal to the sum of the B-field in free space and the magnetization field (M-field):

$$B = \mu_0 (H + M) \tag{2.3}$$

For any material magnetization field M is defined as:

$$M = \chi H \tag{2.4}$$

Where χ is the magnetic susceptibility of the material. It's a dimensionless quantity and signifies the degree of magnetization of a material in response to an applied magnetic field H. From equation (2.2) and (2.3)

$$B = \mu_0 (H + \chi H)$$

$$B = \mu_0 (1 + \chi) H$$

$$B = \mu_0 \mu_r H \tag{2.5}$$

Where, $\mu_r = (1+\chi)$. μ_r is a dimensionless parameter that defines the magnetic permeability of the material relative to that of free space and called relative magnetic permeability of the material.

Susceptibility and relative permeability are functions of applied magnetic field H and the temperature. It is therefore useful to plot a B-H curve for describing the magnetic properties of certain material. Fig 2-5 shows a B-H plot of a typical ferromagnetic material. From the plot it is clear that the magnetic response is not linear. The plot has a linear region at low applied H-field and a saturation region at a higher applied H-field. Ferromagnetic and ferromagnetic materials exhibit hysteresis while demagnetized. Hysteresis is the phenomena where the M-field, as well as the B-field does not return to zero even when the H-field is completely removed. The degree of hysteresis i.e. the strength of the hysteresis is indicated by coercivity. Coercivity specifies the magnitude of the applied H-field that is to be applied in the opposite direction of the B-field to completely cancel the B-field inside the material.

2.5.2 Classification of Magnetism and Magnetic Materials

In general all materials respond to an applied magnetic field to a certain degree. Depending on the behavior of the material under an external magnetic field, magnetic materials can be classified into paramagnetic, diamagnetic, ferromagnetic , ferromagnetic and antiferrimagnetic. This difference in behavior is due to the difference in structure of the material on the atomic and sub-atomic level.

2.5.2.1 Diamagnetism and Diamagnetic Material

Diamagnetism is the property of a material due to which it creates a magnetic field opposite to the applied magnetic field, causing a repulsive effect between the material and the magnetic field. Diamagnetism is generally a weak effect in materials. The materials that exhibit diamagnetism are called diamagnetic materials.

The relative permeability of diamagnetic materials is less than 1 i.e. the susceptibility is less than zero. In other words they have negative susceptibility and are repelled by the applied magnetic field. Since diamagnetism is a weak property, the effect is not very common in everyday life. The order of magnitude of the susceptibility of diamagnetic materials is 10-5. But superconductors are strongly diamagnetic as they have susceptibility equal to -1 and they expel all the magnetic field from their interior.

2.5.2.2 Paramagnetism and Paramagnetic Material

Paramagnetism is a property of material that only exists in the presence of an externally applied magnetic field. Paramagnetism causes materials to weakly attract to an applied magnetic field.

Paramagnetic materials have relative permeability greater than 1, so the magnetic susceptibility is positive. The order of magnitude of the susceptibility is 10^{-3} to 10^{-5}. Paramagnetic materials do not retain any magnetic properties when the applied field is removed. Magnesium, molybdenum, lithium etc are paramagnetic in nature.

Superparamagnetism is phenomena similar to Paramagnetism. Superparamagnetism refers to materials which become magnetized in the presence of an external magnetic field, but become demagnetized as soon as the external field is removed.

2.5.2.3 Ferromagnetism and Ferromagnetic Material

Ferromagnetic materials are strongly attracted by the applied external magnetic field. They have large and positive magnetic susceptibility to an external magnetic field. The order of magnitude of susceptibility of ferromagnetic materials is 10^{12} to 10^{15}. The basic difference between a paramagnetic material and a ferromagnetic material is that, unlike paramagnetic material, ferromagnetic material can retain their magnetic properties even when the applied magnetic field is removed. Iron, nickel, cobalt etc. are some ferromagnetic material.

2.5.3 Ferrofluid

A ferrofluid is a liquid that becomes strongly magnetized in the presence of a magnetic field.

Ferrofluids are colloidal suspension of nano-sized monodomain solid ferromagnetic particles (~ 10 nm diameter) suspended in a carrier liquid, either an organic solvent or water. Ferrofluids have the fluid properties of a liquid and the magnetic properties of a solid. The ferromagnetic nano-particles are coated with a layer surfactant to prevent agglomeration (due to Van Der Waals and magnetic forces). Ferrofluids are superparamagnetic in nature, as they do not retain magnetization in the absence of applied magnetic field [77, 78].

Ferrofluids have diversified technological, biomedical and medical applications [77]. Some of the technological applications are dynamic sealing, as dampers in loudspeakers, heat dissipation from equipments etc. ferrofluids are also used in materials research. Biomedical applications include magnetic drug targeting, hyperthermia, MRI, magnetic separation of cells etc. The toxicity of ferrofluid is very low and can be easily used as a drug carrier for targeting drug delivery [79].

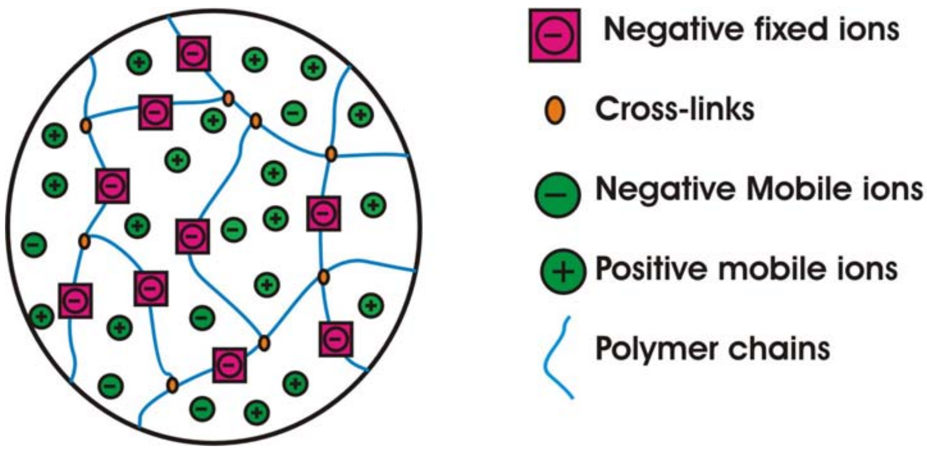

Figure 2-1: Structure of anionic hydrogel [80]

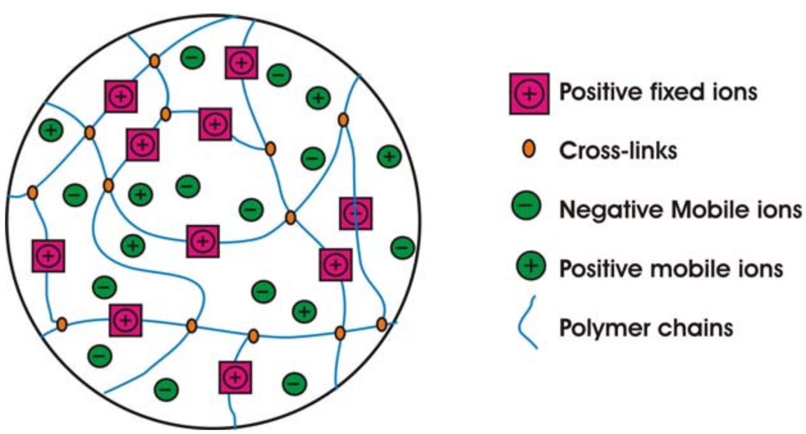

Figure 2-2: Structure of cationic hydrogel [80]

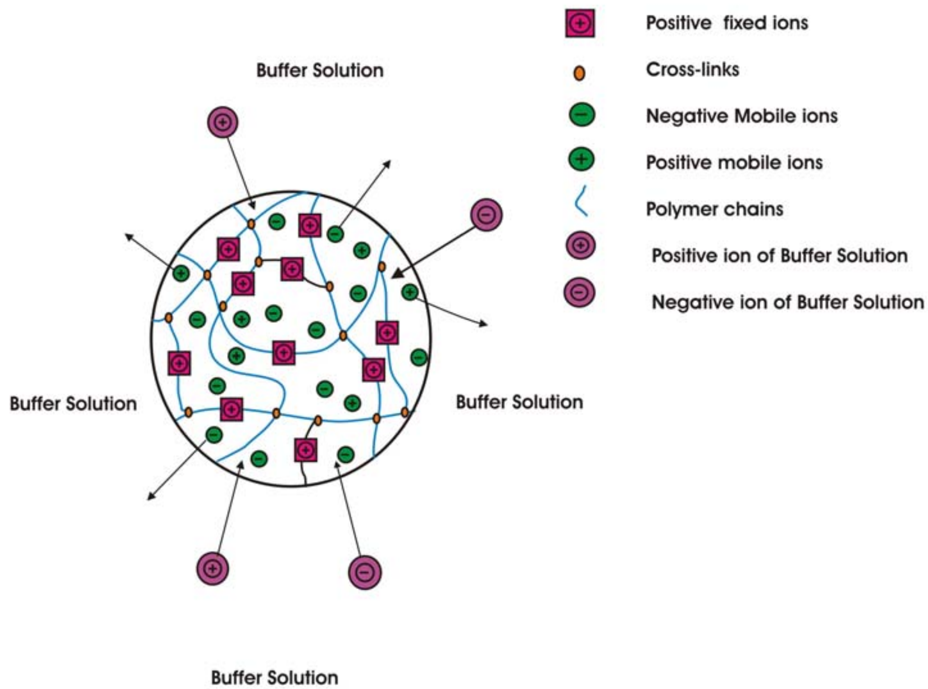

Figure 2-3 Swelling mechanism of Hydrogel by pH stimulation [80]

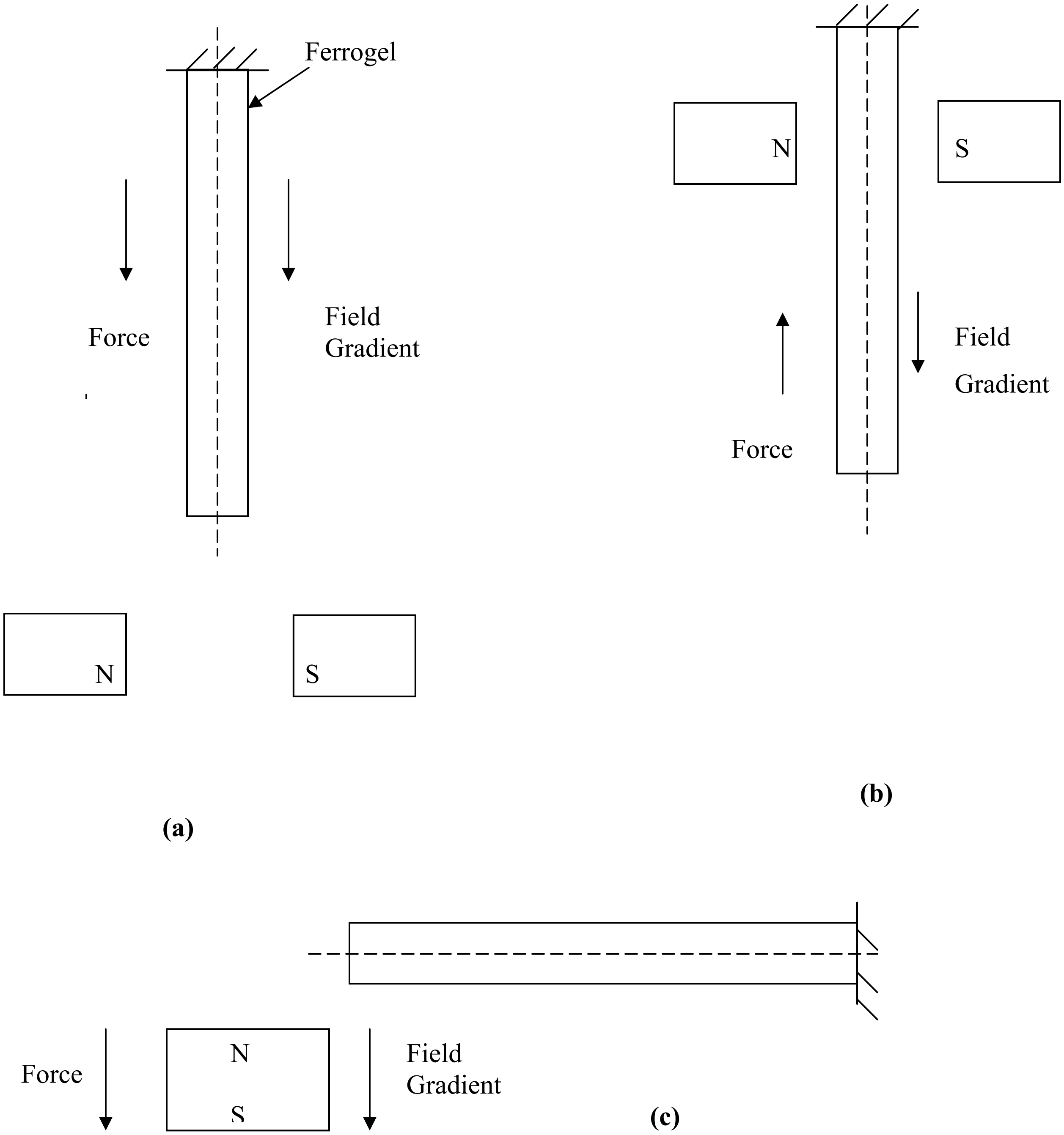

Figure 2-4 (a) Elongation of the ferrogel, field gradient parallel to the gel axis (b) Contraction of the ferrogel (c) Bending of the ferrogel, field gradient perpendicular to the gel axis

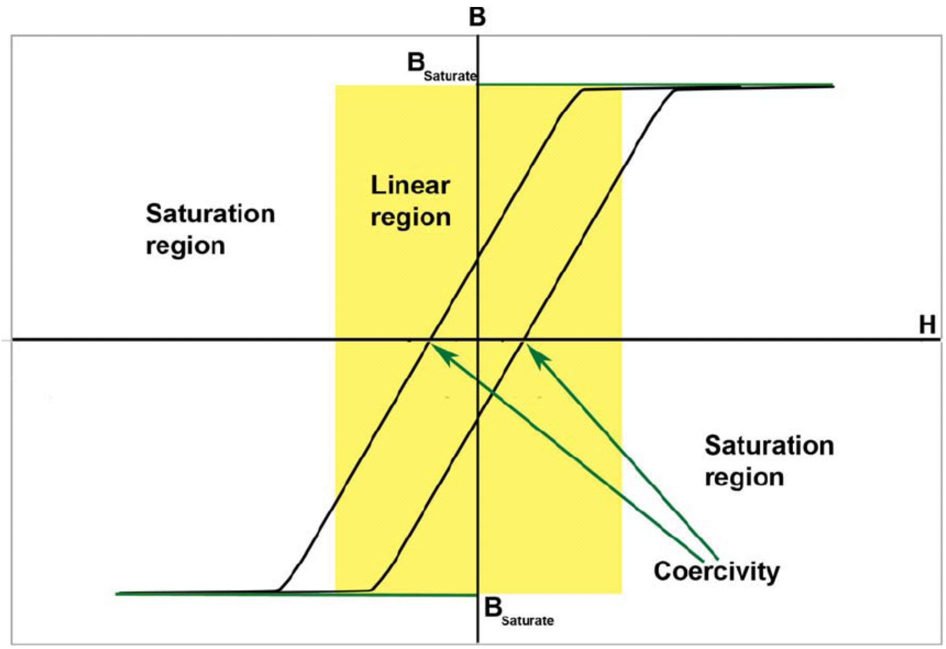

Figure 2-5: B-H plot of ferromagnetic material. The shaded region depicts the linear portion of the curve

CHAPTER 3

MULTIPHYSICS MODELING OF FERROGEL FIBER

3.1 Modeling Approach

In this chapter, a finite element method model of bending deformation of ferrogel microfiber under an applied static magnetic field (created by a permanent magnet) is presented. A coupled structural-magnetic-ALE model is introduced to simulate the bending deformation of a ferrogel fiber.

COMSOL Multiphysics software package is used to simulate the coupled structural-magnetic-ALE model. A positive feedback exists between the magnetic force (exerted by non-uniform magnetic field) and the deformation of the fiber. As the ferrogel fiber is placed in a non-uniform magnetic field, the fiber bends towards the magnet and this bending reduces the gap between the fiber and the magnet. As a result the magnetic force on the fiber increases. The coupled Multiphysics model considers the two-way coupling between the fiber deformations and the magnetic field. It calculates the magnetic force exerted on the ferrogel fiber (magnetic module of COMSOL Multiphysics) and then determines the bending deformation of the fiber caused by the applied force (Structural module of COMSOL Multiphysics). As the ferrogel fiber bends, the geometry of the air domain changes continuously. The arbitrary Lagrangian-Eulerian method (ALE module of COMSOL Multiphysics) solves the Maxwell's equation in the air domain to account the geometry changes associated with the deformation.

3.1.1 Maxwell's Equations

The finite element analysis of electromagnetic problems is done by solving Maxwell's equations subject to different boundary conditions. Maxwell's equations are set of four equations that state the relationships between the fundamental electromagnetic quantities such as magnetic field intensity, electric field intensity, magnetic flux density, electric flux density, current intensity and electric charge density. The four equations are

$$\nabla \times \mathrm{H} = J + \frac{\partial D}{\partial t} \text{ ....Maxwell's Ampere's Law} \qquad (3.1)$$

$$\nabla \times \mathrm{E} = -\frac{\partial \mathrm{B}}{\partial t} \text{ ....Faraday's Law} \qquad (3.2)$$

$$\nabla . D = \rho \text{ ....Electric form of Gauss' Law} \qquad (3.3)$$

$$\nabla \cdot \mathrm{B} = 0 \text{ ....Magnetic form of Gauss' Law} \qquad (3.4)$$

Where

H= magnetic field intensity

E= electric field intensity

B= magnetic Flux density

D= electric flux density/ electric displacement

J= current density

ρ = electric charge density

The following two constitutive relations relate the electric and magnetic flux densities D, B with the field intensities E, H respectively

$$D = \varepsilon_0 E + P \tag{3.5}$$

$$\mathrm{B} = \mu_0 \left(\mathrm{H} + \mathrm{M} \right) \tag{3.6}$$

The model presented in this thesis is a magnetostatic problem where no electric currents are present. In magnetostatic the Maxwell Ampere's law can be written as

$$\nabla \times \mathrm{H} = 0 \tag{3.7}$$

Using the constitutive relation $\mathrm{B} = \mu_0 \left(\mathrm{H} + \mathrm{M} \right)$ and the relation $\mathrm{B} = \nabla \times \mathrm{A}$, (where A is the magnetic vector potential) the equation becomes

$$\nabla \times (\mu_0^{-1} \nabla \times \mathrm{A} - \mathrm{M}) = 0 \tag{3.8}$$

3.1.2 Arbitrary Lagrangian-Eulerian (ALE) Methods

Arbitrary Lagrangian-Eulerian (ALE) is an approach for solving engineering problems which takes the best features of both the Eulerian and Lagrangian approaches [81]. The Lagrangian reference frame, fixes a grid with the material of interest and each individual node of the grid follows the deformation path of the material as shown in figure 3-1(a). Lagrangian approach is mainly used in structural mechanics, as it can map the exact displacement of each particle and thus helpful in tracking the solid motion. Lagragian approach is not suitable for fluid flow problem as the fluid particles usually do not stay together and move indépendly of each other. As a result if a Lagrangian grid is mapped, the fluid particles will not follow the grid path and diverge in the space. On the other hand the Eulerian reference frame is fixed in space and the material deforms with respect to the initial frame as shown in figure 3-1(b). Eulerian approach is mainly used in fluid flow problems. It has the disadvantage that, it can not track the motion of individual particle, so the prediction of motion by tracking individual particle as is done in Lagrangian approach is not possible. In case of large deformation problems in solid mechanics and fluid-structure interaction problems; neither the lagrangian nor the Eulerian approach is suitable. In those cases ALE method is used, as when the grid is distored excessively it adjusts the grid. In ALE method the computational domain is neither fixed as in Eulerian frame of reference nor follow the material deformation as in Lagrangian frame of reference. Rather the grid takes an arbitrary state between those two states as shown in figure 3-1(c).

3.2 Model Overview

In this thesis, the bending deformation of both a straight ferrogel fiber and a stepped ferrogel fiber due to applied magnetic field is modeled.

A straight ferrogel fiber of length L and cross section axa is illustrated in figure 3-2 (a). The fiber is clamped at one end and the other end is free as shown in fig 3.2 (b). The ferrogel fiber is placed in a non uniform magnetic field created by an N48 permanent magnet of size 19.045 mm x 12.7 mm x 6.35 mm. The computational domain is composed of an air domain of 95 mm x 88 mm, an N48 neodymium magnet and a ferrogel fiber as shown in figure 3-3. The length of the fiber was varied from 1000 μm to 4000 μm and the cross section was kept constant, which is 100 μm X 100 μm. The numerical investigation of micro ferrogel fiber was done by varying the aspect ratios (L/a) of the fiber, by varying the volume ratio, v, of the magnetic particle content of the ferrogel fiber and by changing the magnetic field strength. The the maximum tip deformation of the ferrogel fiber was observed for aspect ratios 10, 15, 20, 25, 30, 35, and 40 of the fiber.

The coupled structural-magnetic-ALE model was solved by using the plain strain module, AC/DC module and the ALE module of COMSOL Multiphysics software package. As the ferrogel fiber is placed in a non-uniform magnetic field, it experiences magnetic force towards the magnet and as a result the fiber deforms towards the higher field strength (the magnet). This action in turns increases the forces on the fiber and the fiber deforms more towards the magnet, i.e. a two way coupling exists between the fiber deformation and the magnetic field strength. Because of this two way coupling, the geometry of the air domain changes continuously. Arbitrary Lagrangian Eulerian method was used which solves the

Maxwell's equation in the air domain to account the geometry changes associated with the fiber deformation. The magnetic field was calculated in the surrounding air domain and in the fiber (AC/DC module) by solving Maxwell's equation. The magnetic force; F_{mag} on fiber was calculated by integrating the Maxwell's stress tensor. The built in routine of COMSOL Multiphysics electromagnetic module was used to calculate the force by surface integration of

$$n\mathrm{T} = -\frac{1}{2} H.B + (n.H)B^{T} \tag{3.9}$$

Where H and B are magnetic field intensity and magnetic flux density respectively, and n is the outward normal vector of the boundary. The calculated magnetic force, F_{mag} is applied as the body force on the fiber to observe the deformation of the ferrogel fiber due to the applied magnetic field. The structural displacements (u, v) of the fiber are transferred as a prescribed mesh displacement of the air domain at each iteration of the solution by using ALE method. The ALE algorithm creates a new computational grid based on the fiber displacement (u, v). As the media of ferrogel fiber is the soft material smart polymer hydrogel, large deformation (more than 3%-5% strain) of the fiber was considered. For large deformation problem the non-linear stress strain relation is given by

$$\varepsilon_{ij} = \frac{1}{2}\left(\frac{\partial u_i}{\partial x_j} + \frac{\partial u_j}{\partial x_i} + \frac{\partial u_k}{\partial x_i} \cdot \frac{\partial u_k}{\partial u_j} \right) \tag{3.10}$$

ε_{ij} denotes the strain components and $u_{i,j,k}$ displacement or deformation components. The flow chart of the Multiphysics modeling is shown in the figure 3-4. The model was also solved without considering the geometry change of the air domain (without ALE) and the results for both the cases – with and without ALE were compared.

For drug delivery applications, it is necessary to actuate a ferrogel fiber in its free state instead of clamping at one end as is assumed in the present work. To magnetically actuate a ferrogel fiber toward the application of targeted drug delivery, an attempt was made to break the uniformity of force on the fiber by considering stepped ferrogel fibers. By making stepped ferrogel fiber, the distribution of magnetic particles throughout the fiber was made non-symmetric which in turn ensures non-uniformity of magnetic force throughout the fiber. To compare with the straight ferrogel fiber deformation, a straight fiber of AR 40 were considered and that fiber was made stepped fiber, step by step as shown in figure 3-5.

3.2.1 Material Properties

It is assumed that the magnetic properties of ferrogels and ferrofluids are quite similar [7]. The magnetic moment *m* of the each finely divided magnetic particle in the ferrogel matrix is similar to the molecule of paramagnetic gas. When the ferrogel is subjected to external magnetic field the magnetic moments tend to align themselves with the direction of the field to produce bulk magnetization *M* and are randomly oriented when the external field is removed. The total magnetization of a ferrogel is the sum of the magnetic moment of individual magnetic particles. The magnetization of a dilute magnetic system is expressed by the Langevine function, $L(\xi)$

$$M = nmL(x) = \left(\coth\xi - \frac{1}{\xi}\right) \qquad (3.11)\ [7]$$

Where, n is the number of ferromagnetic particle per unit volume of the ferrogel and the parameter ξ is defined as

$$\xi = \frac{\mu_0 m\mathrm{H}}{k_B T} \qquad (3.12)\ [7]$$

Where H is the applied magnetic field, k_B is the Boltzmann constant, T is temperature, μ_0 is the magnetic permeability of vacuum.

If φ_m is the volume fraction of the magnetic particles in the gel and $M_{s,f}$ is the saturation magnetization of each individual particle. The total magnetization equation of the ferrogel can be written as

$$M = \phi_m M_{s,f}\left(\coth\xi - \frac{1}{\xi}\right) \qquad (3.13)\ [7]$$

The initial magnetic susceptibility is defined as $M = \chi H$ from which

$$\chi = \phi_m M_{s,f} \frac{\mu_0 m}{3k_B} \frac{1}{T} \qquad (3.14)\ [7]$$

If R is the radius of the spherical magnetic particles the moment of each particle can be defined as

$$m = \frac{4R^3\pi}{3} M_{s,f} \qquad (3.15)\ [7]$$

From equation 3.14 it is found that magnetic susceptibility, i.e. magnetic permeability of ferrogel fiber varies with volume fraction of magnetite in the ferrogel. In the present simulation we varied the volume fraction of magnetite content, as a result the value of magnetic permeability also changed.

The ferrogel fibers in the model are made of 2-HEMA hydrogel and ferrofluid. The mechanical properties such as Young's modulus, Poisson's ratio of hydrogel depend on the fabrication condition. The Young's modulus of the ferrogel fiber in the model is 450000 pa and the Poisson's ratio is 0.43. The magnetic permeability of air is 1.

3.2.2 Boundary Conditions

Appropriate boundary conditions are important not only for accurate result, but they also help to decrease the computational complexity by partitioning the area of interest from the rest of the model.

While analyzing the bending behavior of a ferrogel fiber, several boundary conditions were imposed. The boundary conditions of the AC/DC module are: the exterior boundaries of the air domain are magnetically insulated to indicate that normal component of the magnetic flux density is zero i.e. no flux is crossing the boundary. Continuity boundary condition is applied to the exterior boundaries of the magnet and the ferrogel fibers to indicate continuity of the normal component of the magnetic flux density. The ferrogel fiber is structurally fixed at one end and the other three exterior boundaries are free. The numerical model with appropriate boundary conditions is shown in the figure 3-6. The same boundary conditions were used for both straight and stepped fibers. In case of stepped fibers the wider end was clamped and the other end was free as is depicted in figure 3-5.

3.2.3 Mesh Generation

The mesh was created using the standard mesh menu of COMSOL Multiphysics. Free mesh, which is an unstructured mesh network, was used to generate triangular mesh elements. The mesh parameters 'maximum element size' and 'element growth rate' were used to control the mesh size. The maximum element size specifies the maximum allowed size of the element in the computational domain or the boundary. The 'element growth rate' determines the maximum rate at which the element size can grow from a region with small elements to a region with larger elements. A low growth rate means finer mesh distribution in a particular neighborhood. The maximum element size for the magnet, air domain and the ferrogel fibers were set as $0.35e^{-3}$, $2.25e^{-3}$ and $0.05e^{-3}$ respectively. The resulted mesh model with 15224 mesh elements is shown in figure 3-7 for the straight fiber of AR-40. Using ALE To obtain the optimum number of elements, which can provide the required accuracy level of the solution, a mesh sensitivity analysis was performed as shown in the figure 3-8. From the mesh sensitivity plot it is seen that as the number of elements increases the magnitude of deformation decreases and then converged. In case of large deformation analysis distorted elements are produced at the end of the analysis. With ALE framework modeling this problem can be partially overcome. But still there is probability of invertes meshes. The decrease in the value of deformation may be a result of inverted mesh elements. With same element sizes for the three domains as in the case of straight fibers, the number of mesh elements resulted for the stepped fiber is 16416 as shown in the figure 3-9.

3.3 Verification of the Model

To verify the models that are presented in this thesis, the validation of the experimental results of Zrinyi *et al* [6] was done numerically.

Zrinyi *et al*.[6] studied the elongation of the magnetic field sensitive cylindrical hydrogel tubes of approximately 120 mm long and 10-20 mm of diameter in a non-uniform magnetic field. The non-uniform magnetic field was generated by solenoid based electromagnets. The nature of the magnetic field distribution depends on the geometry and quality of electromagnets as shown in the figure 3-10. The strength of the non-uniform magnetic field generated by the electromagnet was varied by changing the steady current intensity in the solenoid. For different current intensity, i.e. for different magnetic field gradient the elongation of the ferrogel tubes was observed.

To compare the experimental results presented by Zrinyi *et al.* [6], a numerical model of a cylindrical ferrogel tube is presented in this thesis. The ferrogel tube is fixed at one end and the other end is subjected to a non-uniform magnetic field (figure 3-10). As the gel tube is placed in a non-uniform magnetic field, the tube elongates towards the magnet and this elongation reduces the gap between the gel tube and the magnet. This in turn increases the magnetic force on the gel tube. That means there exits a two way coupling between the gel tube elongation and the magnetic field as in the case of the bending deformation of the ferrogel fiber that we considered in our present thesis. Arbitrary Lagrangian-Eulerian method (ALE module of COMSOL Multiphysics) solves the Maxwell's equation in the air domain to account the geometry changes associated with the elongation of the gel tube. The elongation that was observed experimentally by Zrinyi *et. al.* [6]. and the elongation that is calculated numerically in the present work are plotted on the same graph as shown in figure 3-11 and an excellent agreement can be observed between the experimental and the numerical results. So, from this comparison we can conclude that, the model that we presented in this thesis for studying the bending deformation of the ferrogel fiber is validated.

3.4 FEM Results

Due to computational limitations, only necessary details were modeled in the FEM of the ferrogel fiber. Two types of fibers were modeled- straight and stepped. The first simulations were a series of models that were used to determine the bending deformation of straight ferrogel fibers by varying the volume fraction of ferrofluid, by changing the magnetic field strength and varying the aspect ratio of the fiber. The second series of simulations were the models of stepped ferrogel fibers to determine the bending deformation by varying the same parameters as in the case of first series of simulation. The boundary conditions that were discussed in section 3.2.2 were applied to simplify the models.

3.4.1 Straight Fiber Models

This section presents the modeling results of straight ferrogel fibers. Figure 3-12 shows the bending deformation of ferrogel fibers as a function of volume fraction of magnetic particle content for aspect ratios 40, 35, 30, 25, 20, 15 and 10. In case of each aspect ratio, as the magnetic particle content increases, the maximum deformation of the ferrogel fiber increases. This is because more magnetic particle content causes the ferrogel fiber to be subjected to stronger magnetic force for the same magnetic field strength.

Figure 3-13 shows the bending deformation of the ferrogel fiber as the function of the aspect ratio and it is found from this plot that maximum deformation of the ferrogel fiber increases non-linearly with the increase in aspect ratio for a certain magnetic field strength as the aspect ratio increases the maximum deformation of the fiber increases. The reason is that, with the increase in aspect ratio the stiffness of the fiber decreases which in turn causes the high aspect ratio fiber to deform more than the lower aspect ratio fibers.

The bending deformation of the ferrogel fibers was also investigated by varying the magnetic field strength for each aspect ratio and each volume fraction of magnetic particle content. Figure 3-14 shows the bending deformation of ferrogel fiber of aspect ratio 40 and volume fraction of 1%. It is found that as the field strength increases the maximum deformation also increases and this variation is linear.

Figure 3-15 shows the plot of bending deformation of ferrogel fiber with and without ALE framework. A significant deviation can be noticed form this plot. In case of the model, without ALE framework, the geometry change of the air domain due to two-way coupling between the fiber deformation and magnetic field strength is not considered, which is far from the physical problem. So the model considering ALE framework is considered reasonable as it accounts the geometry changes of the air domain associated with the fiber deformation.

3.4.2 Stepped Fiber Models

The deformation of stepped ferrogel fibers were investigated and compared with the deformation of straight ferrogel fibers. The simulation was done for each of the stepped fiber using the same boundary conditions as in the case of straight ferrogel fibers. Figure 3-16 shows the plot of maximum deformation vs. volume fraction of magnetic particles for two stepped fibers of length 4000 μm and the straight ferrogel of AR 40. In case of the stepped ferrogel fibers the maximum deformation for each of the volume fraction is higher than the solid straight fiber of the same length. Form the figure, it is found that as the stepped ferrogel fiber resembles towards the straight fiber the bending deformation is also getting closer to that of the straight fiber.

The deformation of the stepped fiber was also investigated by varying the magnetic field strength and the nature of variation was same as in the case of straight ferrogel fibers, i.e. the variation is linear.

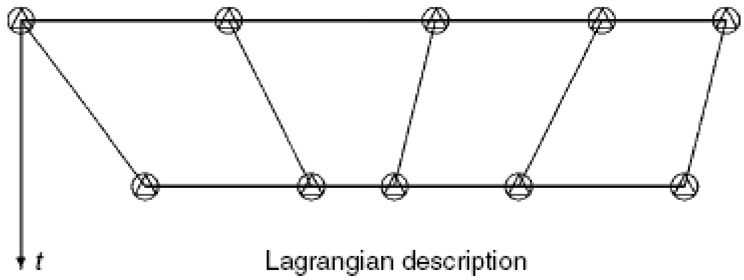

Figure 3-1 (a)[81]

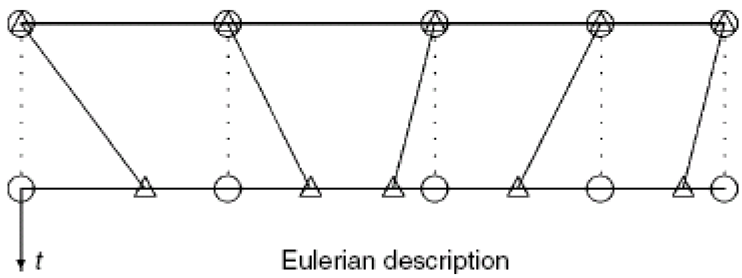

Figure 3-1 (b)[81]

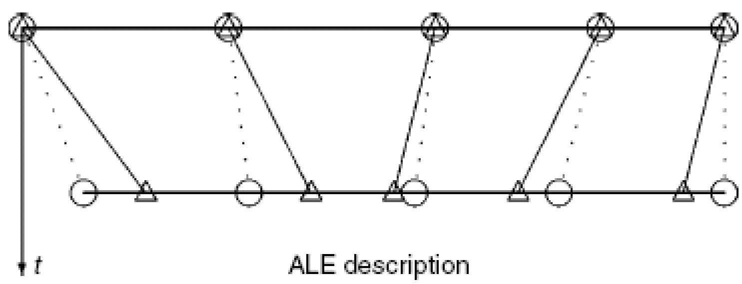

Figure 3-1 (c)[81]

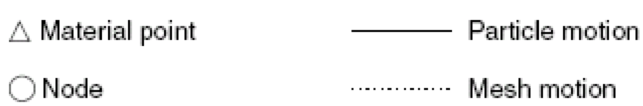

Figure 3-2 (a): A straight ferrogel fiber of length L and cross section axa

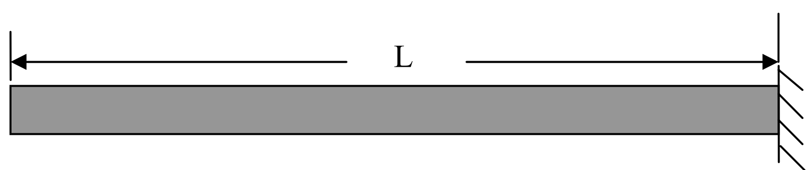

Figure 3.2 (b): 2-D view of a straight ferrogel fiber

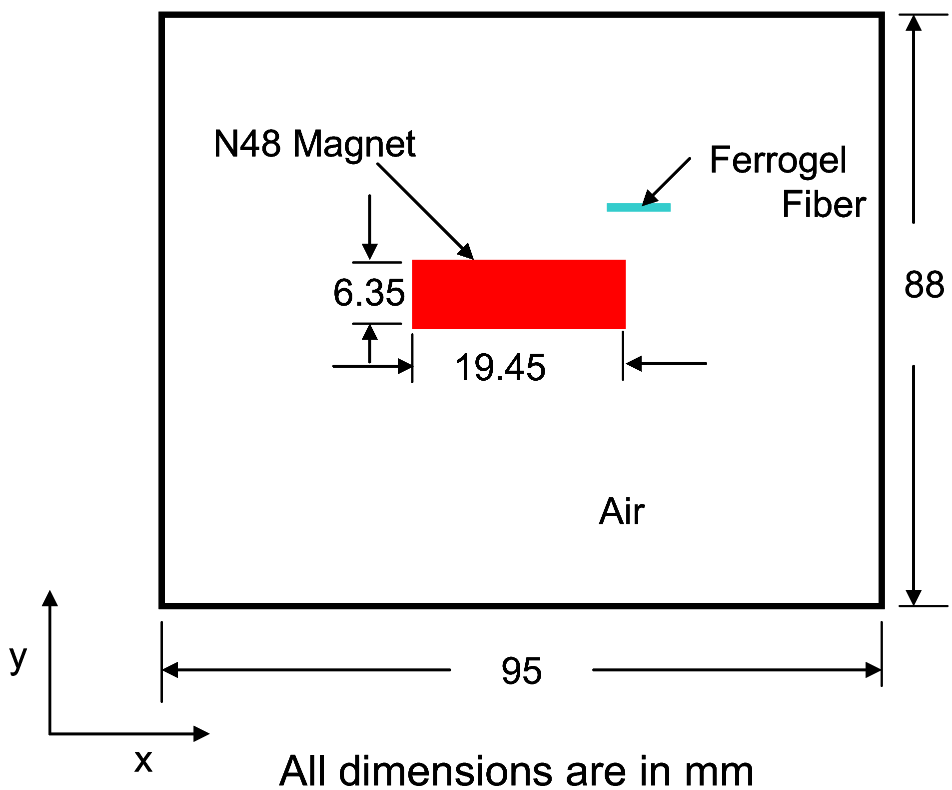

Figure 3-3: Model set-up of the numerical investigation of micro-ferrogel fiber

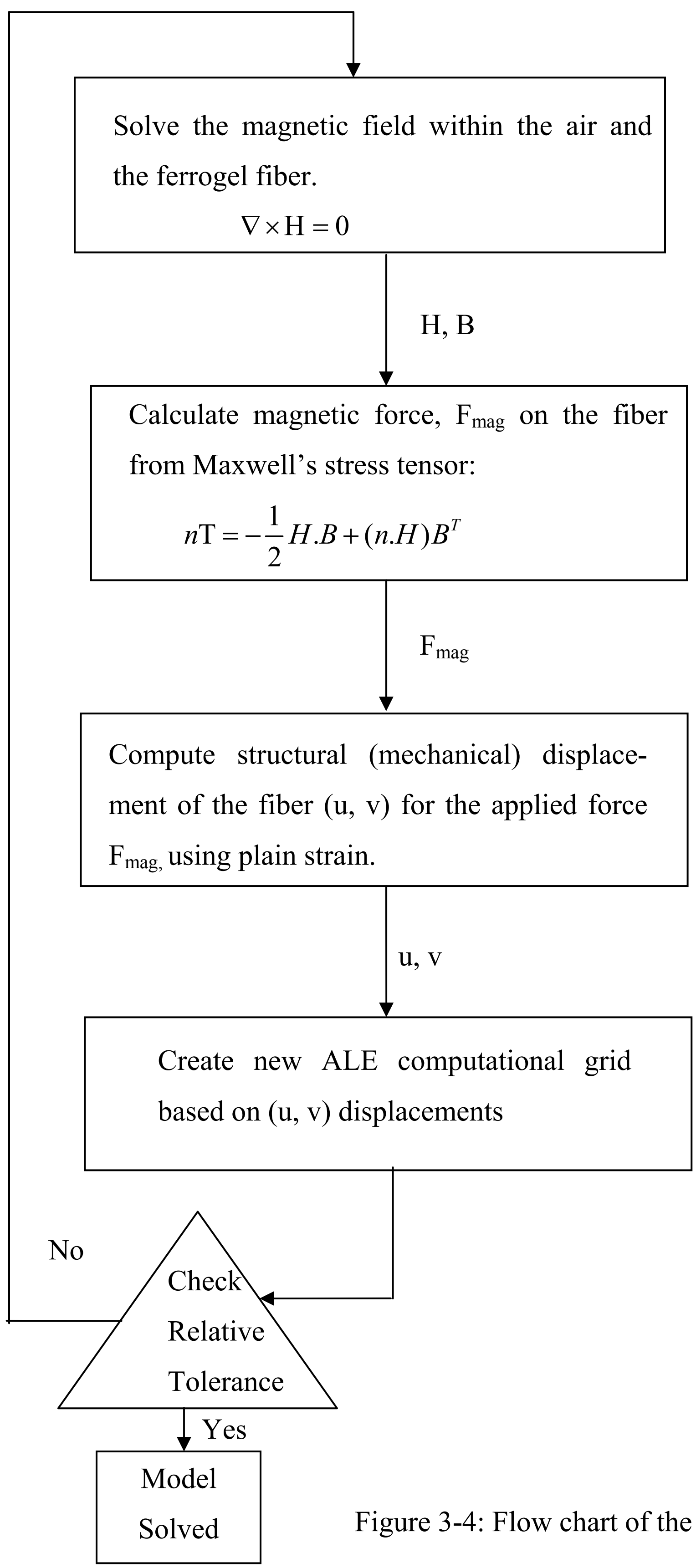

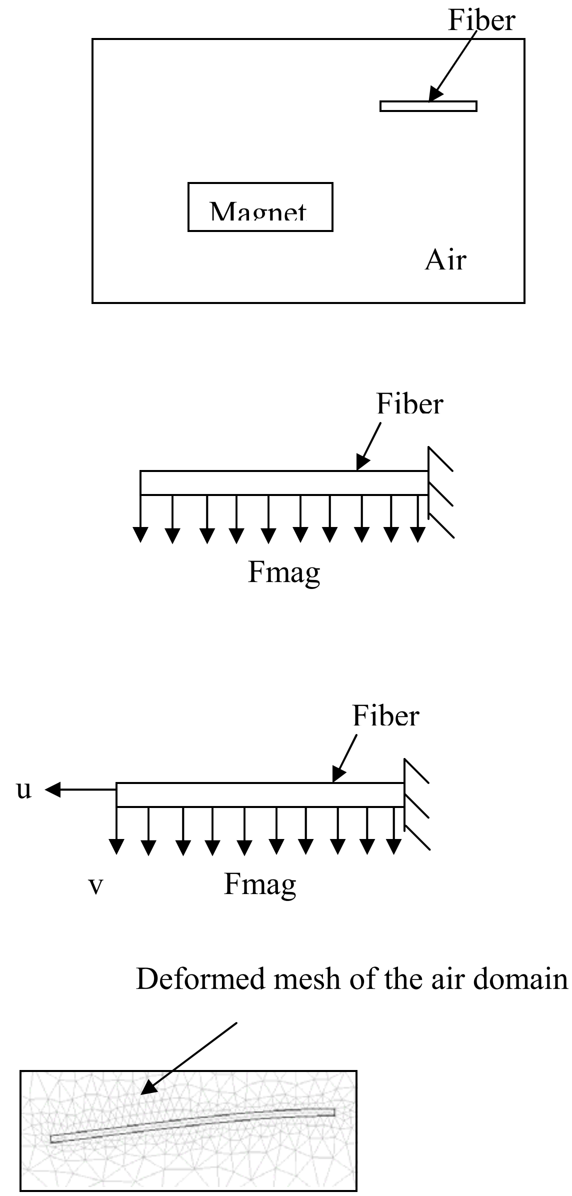

Figure 3-4: Flow chart of the Multiphysics modeling technique of ferrogel fiber

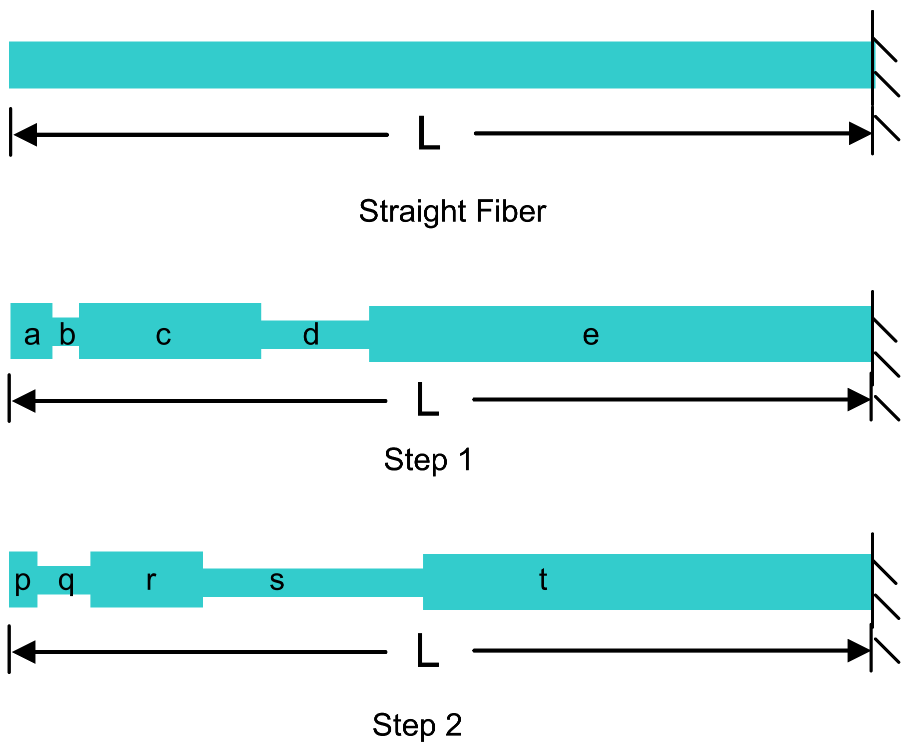

$p= x, q=2x, r=4x, s=8x, t=16x$

$a=1.5x, b=x, c=6.5x, d=4x, e=18x$

Figure 3-5: Steps of making stepped ferrogel fibres from a straight fibre

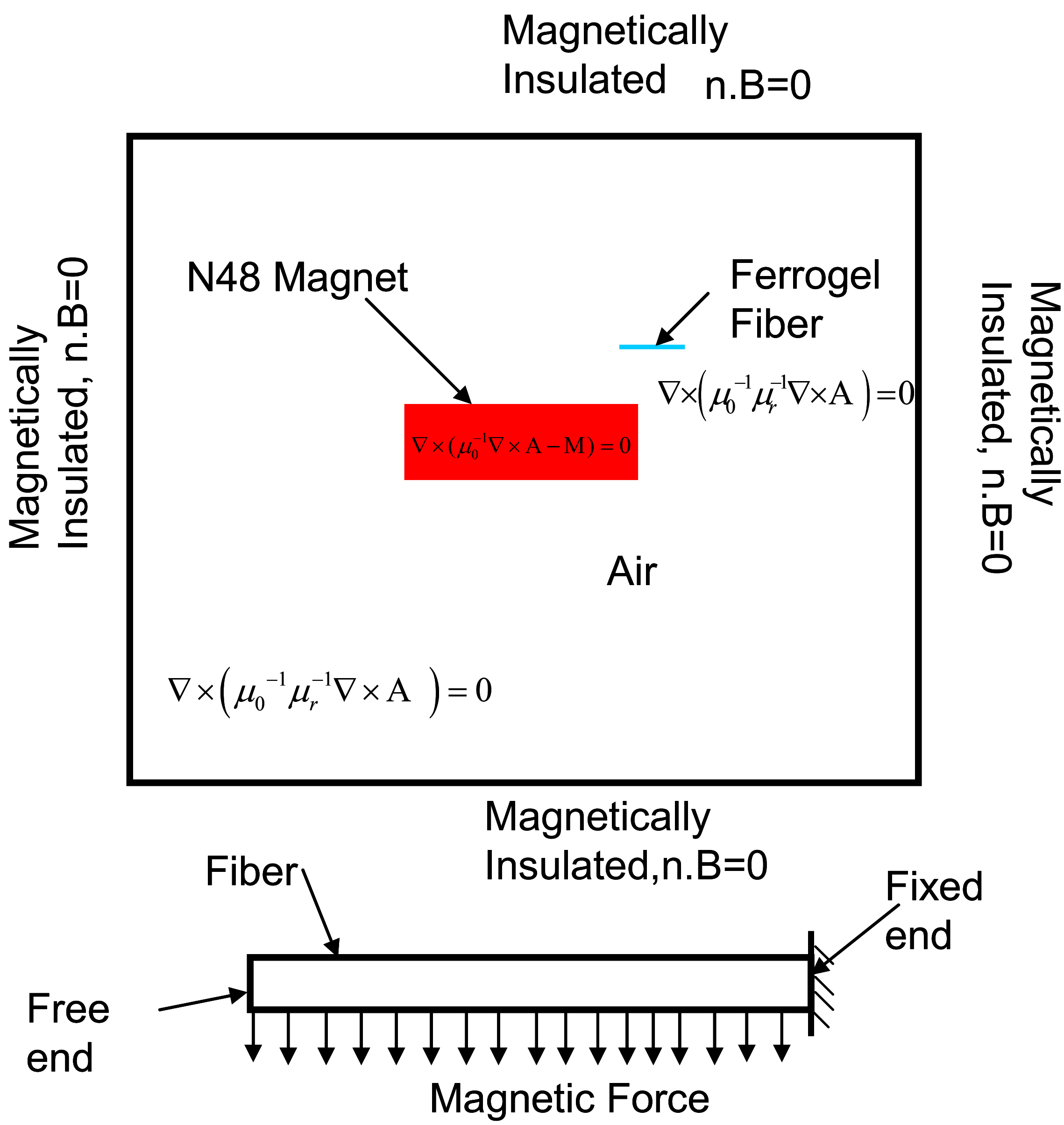

Figure 3-6: The numerical model set-up with appropriate boundary conditions

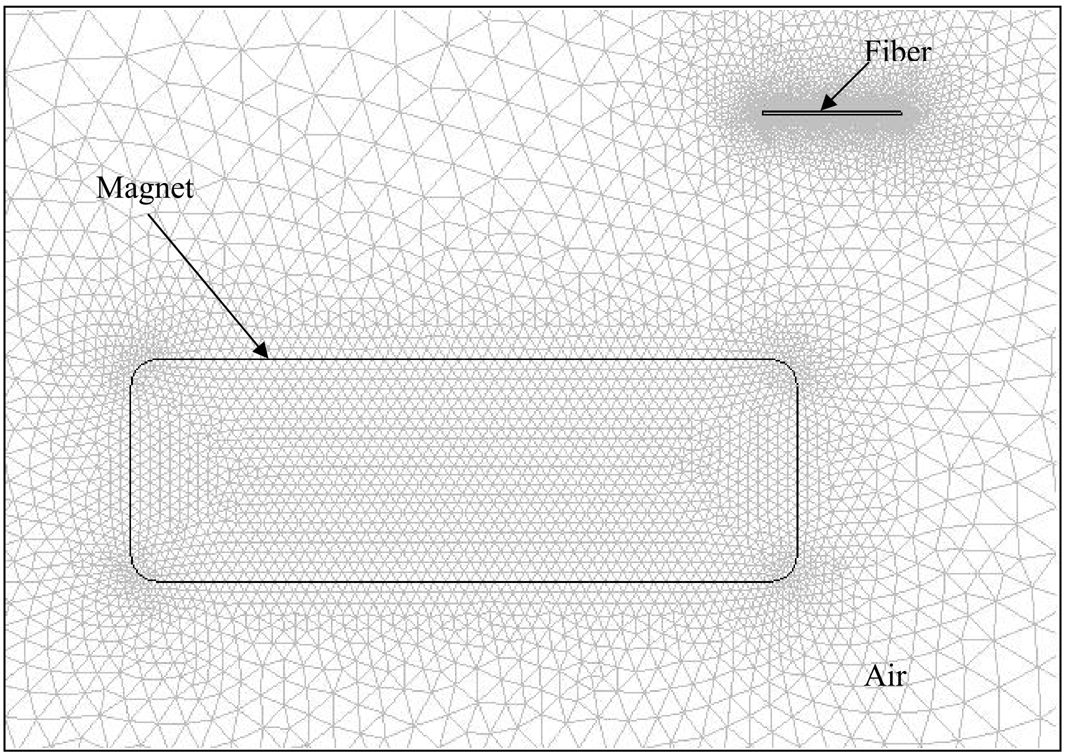

Figure 3-7: The straight ferrogel fibre model with mesh (AR-40), number of elements 15224.

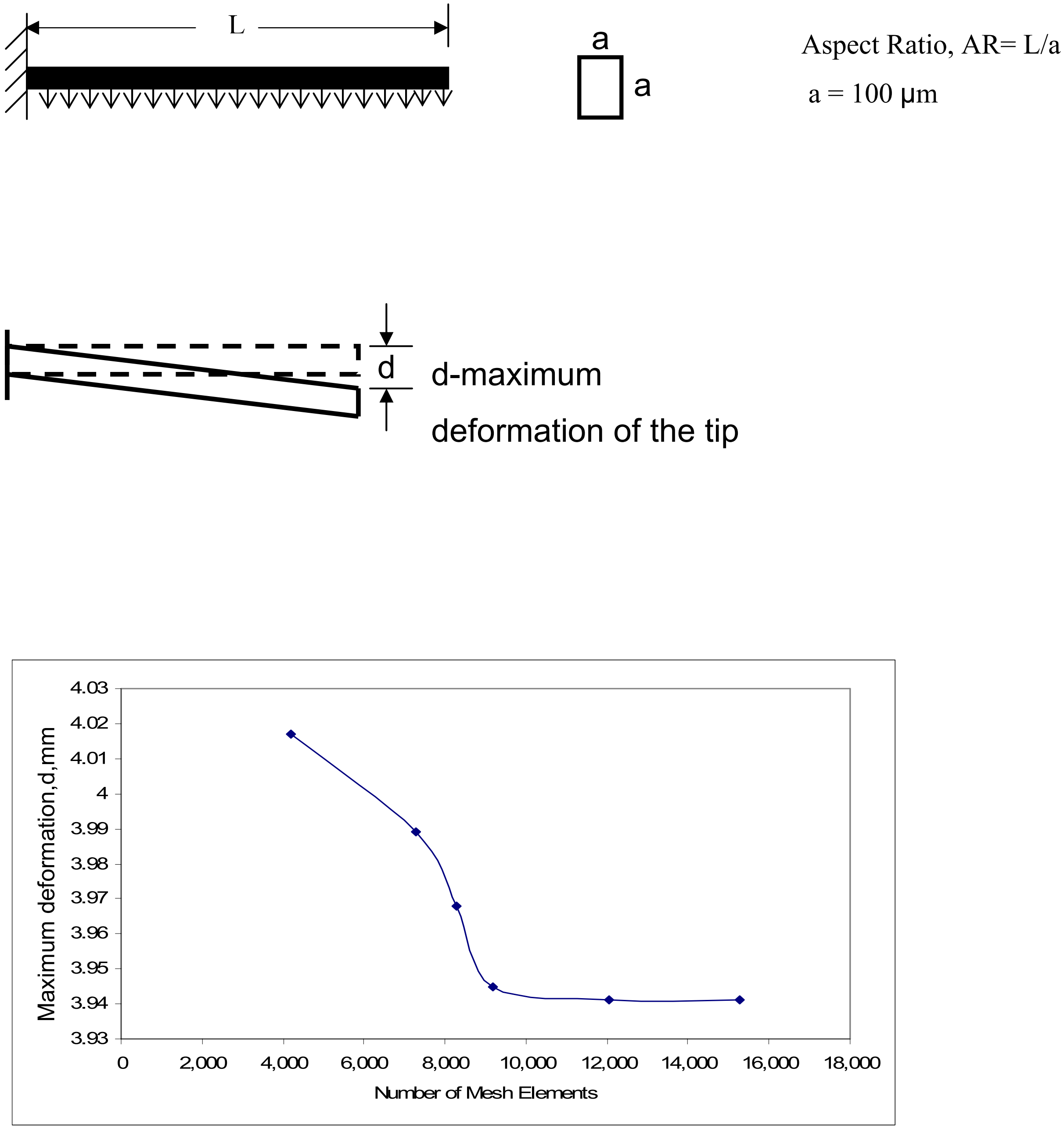

Figure 3-8: Mesh sensitivity test, maximum deformation, d, mm vs. number of elements.

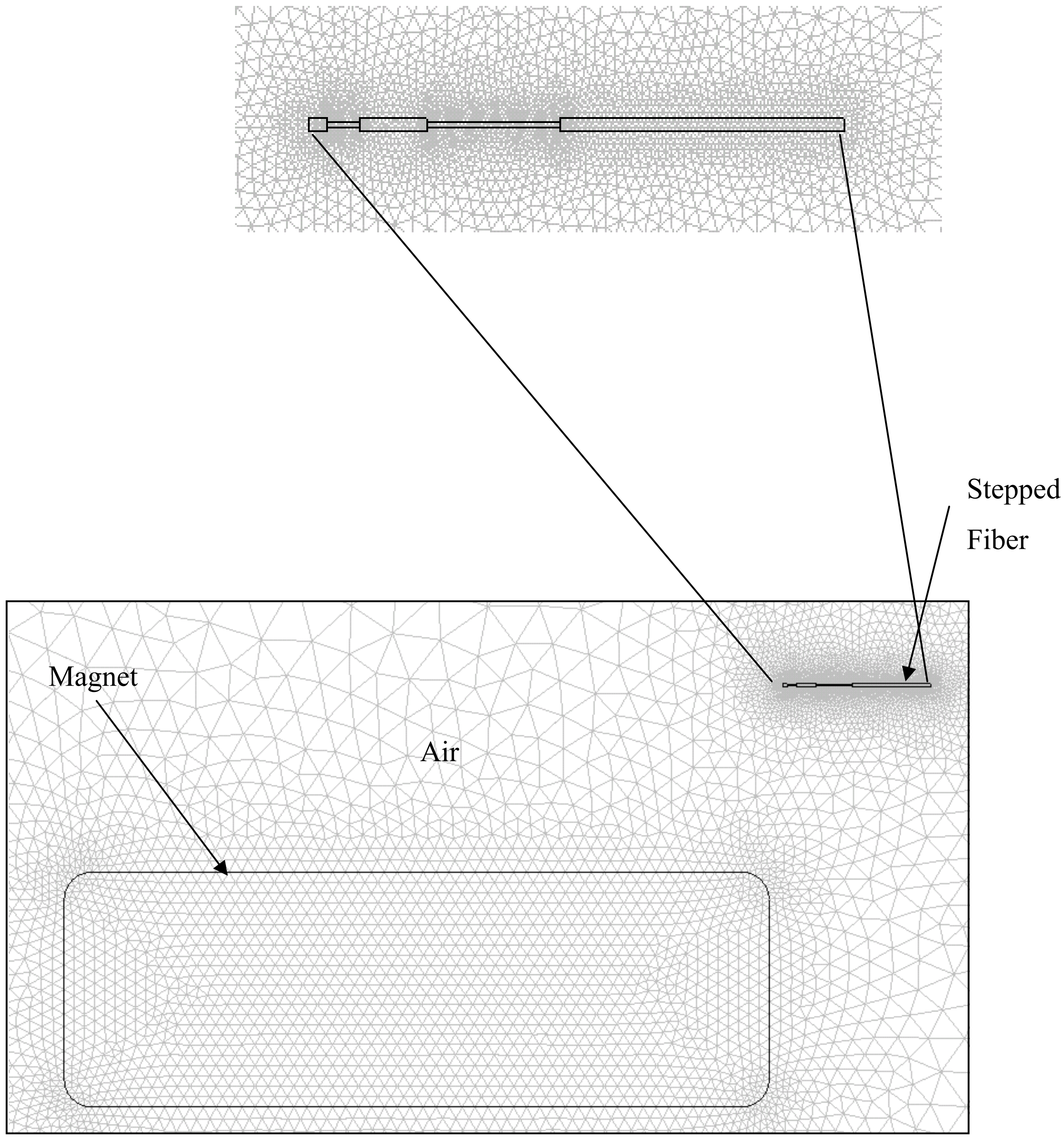

Figure 3-9: Stepped fibre model with mesh (number of elements 16416)

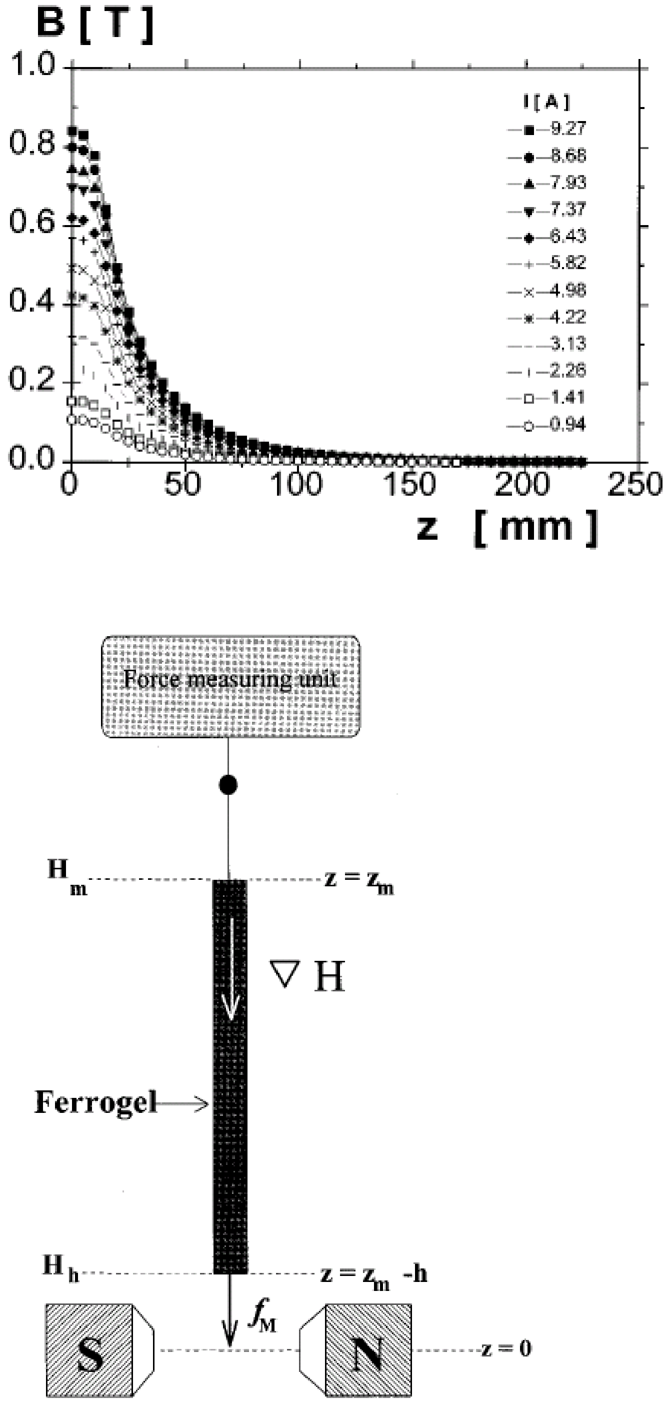

Figure 3-10: The magnetic field strength, B [T] vs. distance z, mm plot for Zrinyi *et al* [6, 8]experiment and the experimental set-up [6].

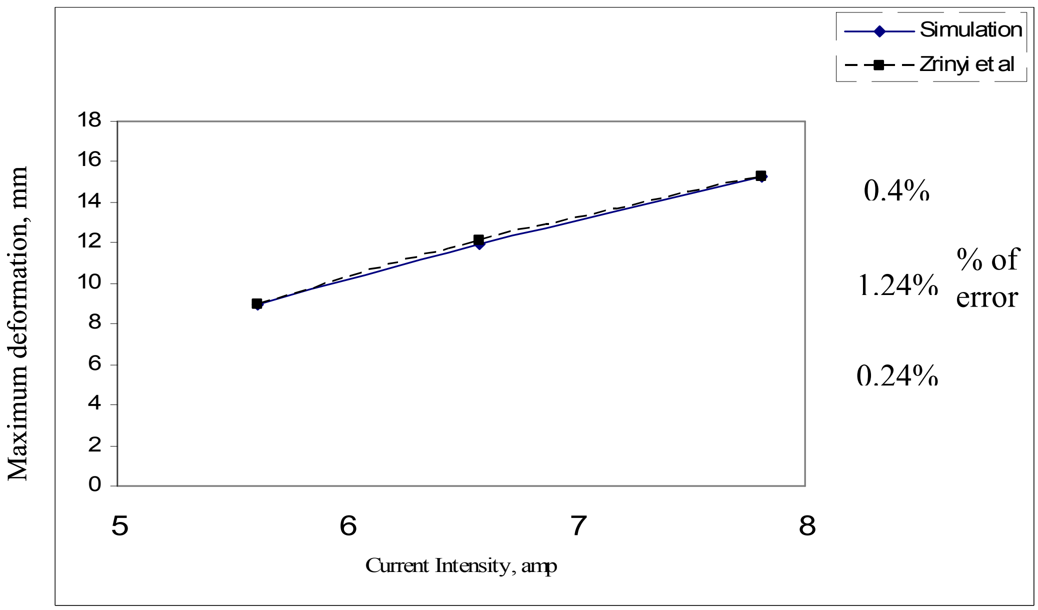

Figure 3-11: Deformation vs. current intensity of present numerical analysis and the experimental results of Zrinyi *et al.*[6]

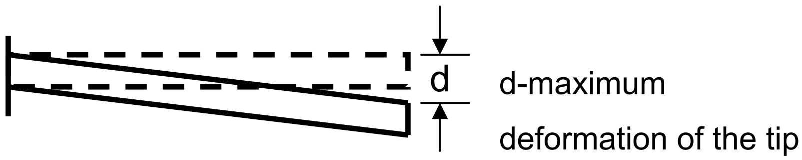

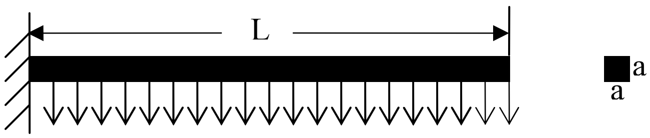

AR= L/a a = 100 µm

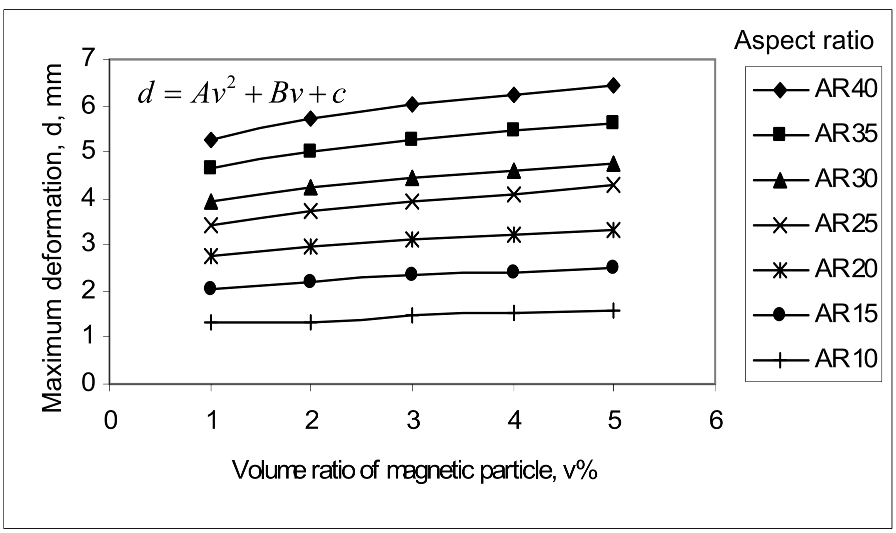

Figure 3-12: Maximum deformation of straight ferrogel fibres vs. volume fraction of magnetic particles for Aspect Ratios 40, 35, 30, 25, 20, 15 and 10. A, B and C are constants

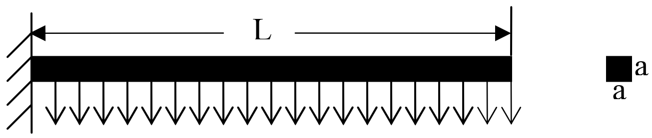

AR= L/a, a= 100 μm

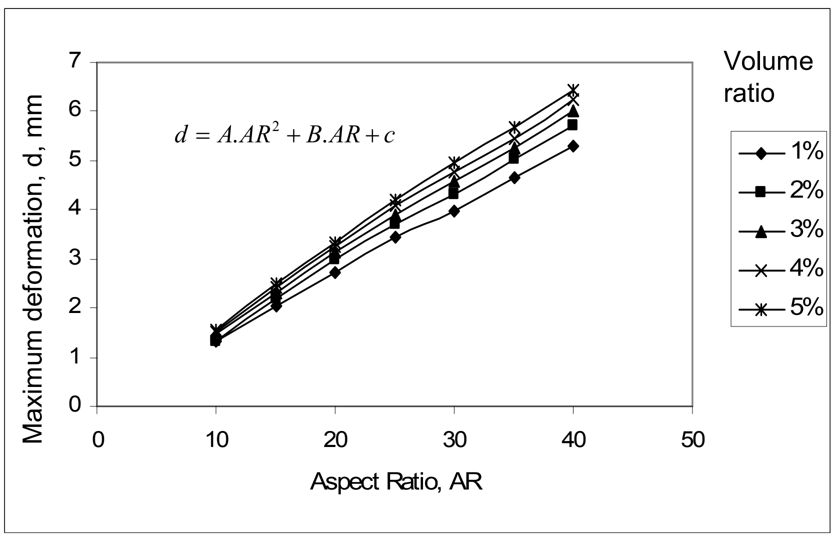

Figure 3-13: Maximum deformations vs. aspect ratio plot for different volume fraction of magnetic particle content of the fibres. A, B and C are constants.

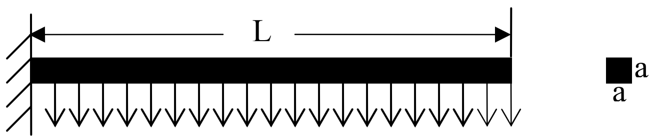

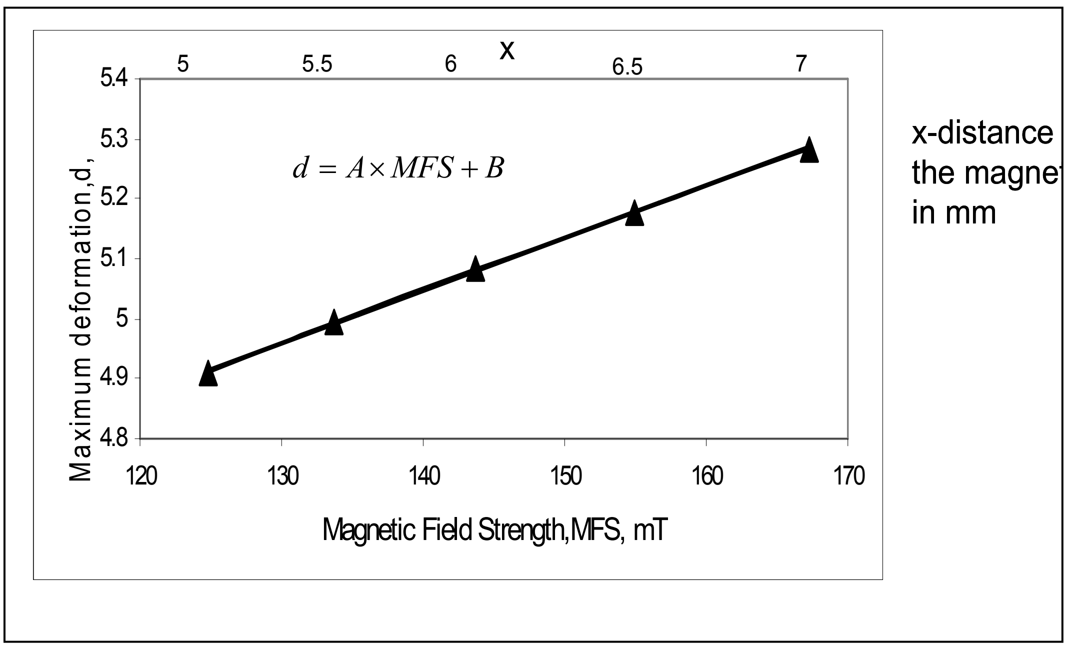

Figure 3-14 Maximum deformations vs. magnetic field strength (AR 40, 1% volume ratio). A and B are constants.

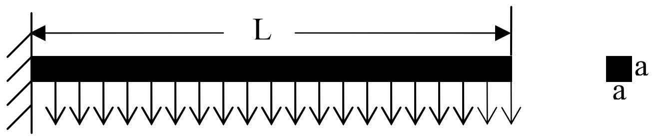

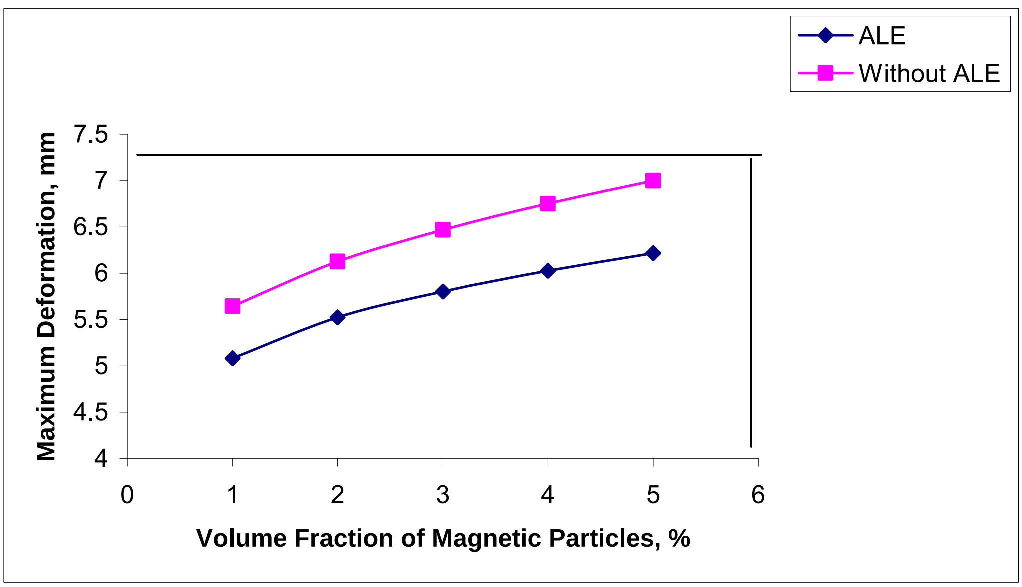

Figure 3-15: comparison of maximum deformation of ferrogel fibers (straight) between the model with and without ALE framework.

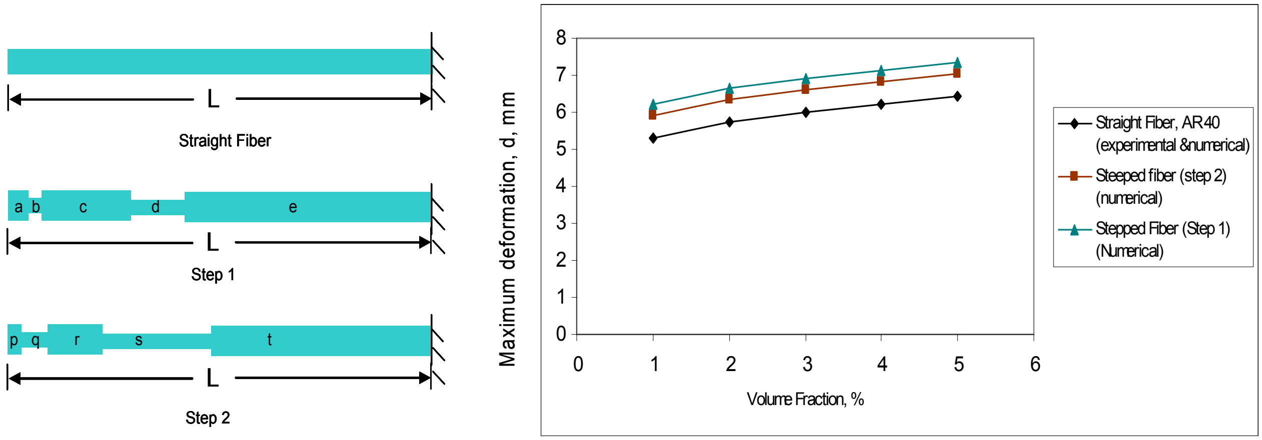

p= x, q=2x, r=4x, s=8x, t=16x

a=1.5x, b=x, c=6.5x, d=4x, e=18x

Figure 3-16: comparison of maximum deformation between stepped and straight ferrogel fibres

CHAPTER 4

FABRICATION OF FERROGEL FIBERS AND EXPERIMENTS

Ferrogel fibers are fabricated and their deformations are observed under applied non-uniform magnetic field. The fabrication procedure of the ferrogel is documented in the following section. Also the problems encountered during the fabrication procedures are discussed. A number of experiments are conducted to observe the deformation of the ferrogels under applied non-uniform magnetic field. The next section of this chapter describes the equipment and materials that were used in the experiments.

.

4.1 Fabrication of Ferrogel Fiber

This section discusses the fabrication technique of micro ferrogel fibers. Fabrication of ferrogel fiber requires micro-beakers. Two types of micro-beakers were used to fabricate ferrogel fibers- glass micro beaker and PDMS (polydimethyl siloxane) micro-beakers. The problem using glass micro-beaker is that, ferrofluid used to fabricate ferrogel leaves dark stain in the beaker and further use of that beaker is not possible sometimes because of that stain. As in the present work, reuse of the beaker was needed; PDMS micro beakers were preferred as the fabrication procedure of PDMS micro-beakers is much easier than that of the glass micro-beakers. The fabrication of PDMS micro-beakers requires a mold/

master with patterns of micro-beakers. The fabrication techniques of the master and micro-beakers are presented step by step in the following sections.

4.1.1 Fabrication of Silicon Master and PDMS Micro Beakers

Silicon master was fabricated using two different methods- silicon etching and SU-8 method. This section describes both the methods and their advantages and disadvantages. In both the methods few steps are common, such as design and photomask generation.

First the desired patterns were designed using CAD software. Next, the design was transferred to a chrome-gold soda lime glass to create a photo mask utilizing a laser mask generator. This photo mask was then used to create the master (mold) on silicon substrates using either SU-8 method or silicon etching process. Finally the Si master was used to cast the micro-beakres by pouring and curing PDMS on them. Both the silicon etching and SU-8 procedure were carried out at the Nanofabrication (NanoFab) facility at the University of Alberta. The following sections provide more details on the intermediate steps as discussed above and shown in figure 4-1 and 4-2.

4.1.1.1 Design

Designing the pattern on the master is the first step after deciding on a manufacturing process. The design of the pattern was created using the L-

Edit®(MEMSPro, USA). Compared to other design CAD software like AutoCad and Pro-E, L-Edit is not as user friendly and is cumbersome to use. Although other Cad softwares could have been used to create the design, there were some problems arising when integrating the design file with the mask generator. This was avoided when the file was generated using the NanoFab prescribed software L-Edit.

4.1.1.2. Photomask Generation

Once the design stage was completed, the outcome of the L-edit program is a file that was compiled for use in the laser pattern generator. The photo mask was produced using a DWL-200 laser mask generator (Heidelberg, Germany). The Heidelberg DWL 200 is a highly precise and accurate instrument using a Krypton-Ion laser to expose at a wavelength of 413 nm. There are generally four steps involved in the creation of the mask: printing, developing, etching and cleaning. The machine prints the patterns by raster scanning blank 5 inch soda lime glass squares (thickness 0.09 inch, Paragon Optical Company, USA) that are coated with chrome and 530 nm of AZ 1518 photo resist. A minimum feature size of 0.7 – 0.8 μm can be attained using the laser mask writer, depending on the geometry of the feature. Once the mask blank has been exposed by the Krypton-Ion laser, photoresist exposed to the laser is chemically altered so that when it was agitated in a developer, that part of the photoresist washed away. This revealed the pattern that was designed in the CAD program. After developing, the mask blank therefore had both the bare chrome and the unexposed photoresist on it. The photoresist acts as a protective layer so that when the mask was placed in chrome etch, only the uncovered chrome was removed. Once the developing and etching was finished, it was necessary to properly clean the mask before using it in lithography. The mask was inspected and the photoresist stripped using acetone and IPA followed by a 30 min dip in a cold piranha bath.

4.1.1.3. Silicon Master by Etching

Following are the steps to fabricate silicon master by silicon etching:

4.1.1.3.1 Cleaning

The Si wafer was cleaned thoroughly .Cleaning was carried out by soaking the Si substrates in freshly prepared Piranha solution which contains 75% H_2SO_4 and 25% H_2O_2, by volume. The mixing procedure produces a significant amount of heat, raising the temperature of the solution to about 110°C. The substrates were immersed in this hot solution for 15 min. This guarantees that all organic contaminants will be removed. Once removed from the Piranha solution, the substrates were rinsed in copious amount of deionized water and dried in N_2.

4.1.1.3.2 Thermal (Silicon dioxide) Layer Growth

Next the wafer was placed in a furnace to form a layer of silicon dioxide (SiO_2) before spin coating it with the resist. This “buffer” or “masking” layer of oxide is required for the later deep reactive ion etch (RIE) etching process. The thickness of the layer depends on the depth to which the substrate will be etched. For example, for our Si master, a 0.5 μm oxide layer is required for a maximum etch depth of up to 100 μm depth of the pattern. The wafers were placed in a furnace for 6-7 hours at 900°C to obtain a 0.5 μm thick oxide layer. The substrate was allowed to cool and a thin adhesion promoting layer of HMDS (hexamethyl disilazane) was coated on top to promote good adhesion for the resist. The HMDS reacts with the oxide surface in a process known as silylation, forming a strong bond to the surface. At the same time, free bonds are left which readily react with the photoresist, enhancing the photoresist adhesion.

4.1.1.3.3 Spin Coating Resist and Soft Bake

Spin Coat: The patterning process begins with spinning the photoresist. Photoresist is a polymer sensitive to UV light. It changes its chemical composition once exposed to UV light. The photoresist used in this process was a low viscosity resist HPR 504. The substrate was placed on a spinning machine and about 5 ml of the resist was dispensed at the centre of the wafer and spread at 500 rpm for 10 s. After the initial spreading, the actual spin that coats the resist on the substrate was performed at 4000 rpm for 40 s.

Soft Bake: After spinning, the wafer with the wet HPR 504 layer was then baked on a hot plate to dry and stabilize the film. This pre-exposure bake also makes the surface non-sticking, which prevents it from leaving remains on the photo mask. The duration of baking depends on the type of resist. For glass substrates covered by a thin HPR 504 resist, baking at 110°C for 90 s on a hot plate is recommended. After the bake, the resist was cooled for about 15 min before the exposure step.

4.1.1.3.4 Exposure and Development

Exposure: Once the resist was baked, it was ready for exposure. The exposure process started with setting the mask generated on a mask aligner tool. It was important to ensure that the photo mask was clean before mounting on the machine. Once the mask was mounted, the wafer or Si substrate was placed on the substrate holder by turning the vacuum on. Next the mask was aligned and centered with the Cr side facing towards the Si substrate, which is positioned properly beneath it. After alignment, the substrate was brought into contact with the mask. At this stage it was crucial to ensure that the substrate did not move or change position once contact was made with the mask, otherwise the alignment would have to be performed again. It was also important to ensure that the mask and the substrate were in good contact. Any trapped particle or debris could potentially create a gap between the mask and the substrate. This would let diffused light penetrate under the mask, thereby, causing a deformation of the features or partial exposure of some parts. The exposure time is dictated by the smallest dimension present on the mask. For our design, the exposure time was generally between 2 to 2.5 seconds.

Development: Developing the photoresist is a chemical process, in which the exposed substrate is immersed in a developer. The developer dissolves the UV exposed parts of the photoresist revealing the bare regions of the Si substrate while leaving the substrate covered with unexposed photoresist. The standard developer for HPR 504 is the 354 Developer. For slower and more accurate processes involving very small dimensions, water can be added to dilute the developer (up to 50% by volume). The standard development time for the resists mentioned above is 20 to 25 seconds in 100% of 354 Developer. However, the developing time may vary; depending on the pattern dimensions, temperature, and humidity. For our pattern dimensions, the developer was diluted and the exposure time varied from 15 to 18 s. Finally the wafer was inspected under a microscope to check for the quality of the whole patterning process after developing the resist. The substrate was subsequently rinsed with de-ionized water and blown dry using N_2.

4.1.1.3.5 RIE (Reactive ion etching)

The next step was to remove the oxide layer from the uncovered regions of Si wafer where the etching action will take place to form the relief pattern or mold. For this purpose, a Buffered Oxide Etch (BOE) was performed with the etching time varying depending on the thickness of the oxide layer. The etching solution contains 10:1 ratio of ammonium bifluoride (NH_4HF_2) and hydrofluoric acid (HF) by volume with an etch rate of 550 Å per minute. The wafer was placed in this solution for about 4 min to remove the oxide layer.

4.1.1.3.6 Dry Etch - BOSCH® Process

In the final step of the master fabrication, an anisotropic etching method was employed for fabricating the relief pattern on the Si master. To achieve anisotropic etching, a Deep Reactive Ion Etch (DRIE) machine using the Bosch® process (named after the German company Robert Bosch that filed the original patent) was employed. This process is used where deep, vertical-walled, high aspect ratio structures with small feature sizes are required. The process cycles between two steps:

Polymer deposition phase: In the deposition stage (typically 10 s long), C_4F_8 (octafluorocyclobutane) gas is introduced in the reactor. The entire surface of the wafer is subsequently coated with Teflon-like polymer formed in the plasma from the C_4F_8 gas.

Etch phase: In the etch phase (typically 15 s), the C_4F_8 is turned off and SF_6 (sulfur hexafluoride) is let into the chamber. The polymer (on the horizontal surfaces of the wafer) is immediately sputtered away by the SF_6 plasma, and then etches the Si below the polymer. The SF_6 etch occurs only on the horizontal surfaces and not the sidewalls, thus producing an almost vertical wall.

A single process cycle etches trenches from 0.5 to 1 µm at an etch rate of 0.5 to 2.0 µm/min (depending on the etch recipe). The cycle was repeated until the desired structure (depth) has been etched. The system was fully computer controlled in all aspects of the pumping cycles and process control, and can be programmed by the user. A masking layer of 0.6 µm thermal oxide (SiO_2) is usually sufficient for about 200 µm deep etches. In this experiment, there four-BOSCH cycles sufficed to obtain the design etch depth of 100 µm with a masking thermal oxide layer of 0.5 µm

4.1.1.4 Silicon Master Fabrication by SU-8 process

Following are the steps to fabricate silicon master by SU-8 method. The clearing of the silicon wafer is done as the same way as is described in section 4.1.1.3.1

4.1.1.4.1 Dehydration Bake

After cleaning the dried wafers was dehydrated so that any water molecules on the substrate surface are evaporated. Wafers were placed on a hot plate at 200^{o}C for 5 minutes. After dehydration the substrate was allowed to cool to room temperature. If cooling is not performed the SU-8 could be thermally cross-linked during spinning.

4.1.1.5 Spin Coating and Soft Baking

Wafers were then coated with a film of SU-8 using a conventional spin-coater. Various film thicknesses can be achieved by changing the RPM of the spin-coater. When pouring SU-8 onto the wafer surface before spinning ensure no air bubbles get trapped beneath the surface or these bubbles could cause feature defects. After spinning the wafer was allowed to sit for 5 minutes, this allows any stresses formed during spinning to relax and the SU-8 has time to reflow forming a smooth surface

The wafers were then placed on the hot plate for a soft-bake. The soft-bake occurred in two stages, first the substrate was baked at 30^{o}C for 1 minute and then the temperature was stepped up to 60^{o}C for 6 minutes. Soft-baking at a lower temperature allows a more controlled solvent evaporation rate, which promotes increased substrate adhesion, increased coating fidelity, and decreases the edge bead. In addition, soft baking at a higher temperature will induce higher internal stresses in the SU-8, which form as the temperature drops. Internal stresses are also caused by the evaporation of the solvent. As the solvent is evaporated the total SU-8 volume decreases, which causes stresses to form between the rigid silicon substrate and the shrinking SU-8. After soft-baking the wafer was allowed to slowly cool to room temperature for 2 hour.

4.1.1.5.1 Lithography

The soft baked wafers were then exposed to UV light for 3 seconds using an AB-M mask aligner. Exposing SU-8 to UV light caused the photoinitiator molecules to transform into acids. These acids are essential to the cross-linking mechanism which occurs during the post-exposure bake. SU-8 has very high optical transparency above 360 nm and has low UV absorption, which allows for easy irradiation of thick films.

4.1.1.5.2 Post Exposure Bake

After UV exposure a post exposure bake (PEB) of the SU-8 was carried out on a standard hot plate. The wafer was baked at 30^{o}C for 1 minute, then the temperature was stepped up and baking occurred at 60^{o}C for 6 minutes. This PEB causes acid molecules to react with SU-8 epoxy side groups; this reaction causes radicals to form. These radicals are attached to the SU-8 molecule and react with each other to cross-link the SU-8 molecules together. A low PEB temperature is used to reduce the internal stresses and decrease subsequent cracking of the SU-8. A higher PEB temperature, such as 95^{o}C as recommended by the manufacturer, and could cause long or infinite developing times. The substrate was cooled slowly for 10 minutes before development.

4.1.1.5.3 Developing

The SU-8 coated wafer is then immersed in slightly agitated SU-8 developer, with complete developing occurring in 3-4 minutes. After completion the wafer was removed and rinsed with IPA solution and dried with N_2. If a white film or white spots appear after drying, some of the SU-8 is underdeveloped and should be immersed in developer for a longer time period.

4.1.1.6 Cast Molding

The cast molding process is depicted in figure 4-2. After the master mold was produced, an anti adhesive surface treatment was required before the master could be used to cast the PDMS micro beakers. The surface treatment was needed to favor the release or demolding of the micro-beakers by reducing the surface energy of the Si surface so that the beaker could be removed without tearing or damaging the delicate micro beaker structures. To make the surface anti adhesive, 1H, 1H, 2H, 2H perfluorooctyl trichlorosilane (Aldrich, USA) was used. The substrate and a vial containing a few drops of trichlorosilane were placed in a desiccator under vacuum for 1.5 h. Trichlorosilane evaporates under vacuum and forms a thin layer of hydrophobic coating on the surface of the master.

The micro beakers were cast using polydimethyl siloxane or PDMS which is normally supplied as a two part kit: a liquid silicon rubber base (i.e. a vinyl-terminated PDMS) and a catalyst or curing agent (i.e. a mixture of a platinum complex and copolymers of methylhydrosiloxane and dimethylsiloxane). In the casting step, PDMS polymer was made by combining a 10:1 ratio of Sylgard 184 Base and Sylgard 184 Cure (Dow Corning, Midland, MI) and stirring rigorously until they are thoroughly combined. After the mixing, the mixture will be full of air bubbles and requires degassing because the presence of air bubbles can cause unwanted cavities in the PDMS structure. Degassing was performed by placing the mixture under vacuum (~22 in Hg vacuum) until the bubbles disappeared. The mixture was then poured in the middle of the wafer over the relief structure on its surface from a low altitude (to minimize the risk of trapped air) and allowed to spread. The master was kept horizontal while the PDMS was being poured to ensure uniformity of the thickness of the PDMS micro-beaker formed. The wafer was then baked at 80°C for 2 h causing the PDMS to solidify. Once fully cured, the PDMS was removed from the oven and allowed to cool to room temperature. The micro beakers were then manually stripped off from the master and cut into small individual pieces. The master can be used several times to mold the micro-beakers without compromising the integrity of the beaker structures.

4.1.1.7 Ferrogel Fabrication Procedure

2-HEMA hydrogel, which is also a pH sensitive hydrogel, was used to fabricate ferrogels in the present work. The following steps are used to fabricate the ferrogel fibers:

Step1. At first the 2-HEMA hydrogel ingredients are mixed together. The constituents of 2-HEMA hydrogels are 1. Acrylic Acid (AA) and 2-hydroxy-ethyl-meth-acrylate (2-HEMA) 1:4 molar ratio, 2. Crosslinker: Etheylene-glycol-di-meth-acrylate (EGDMA) (1.0 wt%), 3. Photoinitiator, Irgacure 651:2,2-dimethoxy-2-phenyl-acetophenon(DMPA)(3.0 wt%).

Step 2. After mixing the ingredients together waited for 30 minute to ensure that all the material are well dissolved and mixed in the solution. A piece of metal was sued to stirring to accelerate the mixing process. the mixed precursor was kept away of any UV light source to avoid any unwanted polymerization.

Step 3. Then ferrofluid is mixed homogeneously with 2-HEMA hydrogel precursor in the appropriate volume ratio in a glass beaker. The PDMS micro beaker of the desired fiber shape and size were selected and was sealed with thin PDMS layer. The precursor and ferrofluid mixture are then injected into the beaker through the PDMS layer using syringes.This process was done far from the microscope area.

Step 4. The sealed micro-beaker with the precursor is then aligned with a photomask containing the desired hydrogel shapes using the aligning markers located on the corners of each beaker. The set up is shown in figure 4-3 micro petitioners were used to raise low and rotate the mask until good alignment with the sealed micro-beakers.

Step 5. After aligning the mask and the micro-beaker, the ferrofluid and precursor mixture was exposed to UV light of intensity 35 cm mW/cm2 for 120 sec. The distance from the mask to the UV light guide (from the UV light source) was adjusted to get the desired light intensity.

Step 6. After photo polymerization was done, the un-polymerized precursor was flushed out by clean water.

4.2 Experiment

A number of experiments were conducted on the ferrogel fibers to observe their deformation under the applied magnetic field. Straight ferrogel fibers of aspect ratios 40, 35, 30, 25, 20, 15 and 10 were fabricated by the fabrication method, mentioned in the previous sections. The length of the fibers varies from 1000 to 4000 μm. They have a constant cross-section of 100 μm X 100 μm. Fibers of each aspect ratio were fabricated for 1%-5% volume fractions of ferrofluid. For each volume fraction, the bending deformation of the fiber was investigated experimentally for varying magnetic field strength.

4.2.1 Experimental Setup and Procedure

A very simple experimental set-up was used to investigate the bending deformation of the ferrogel fibers. An N48 permanent magnet of size 19.045 mm x 12.7 mm x 6.35 mm was used to create the desired magnetic field to deform the ferrogel fibers. The magnetic filed strength was measured using a digital gauss meter.

To determine the bending deformation of a ferrogel fiber at a certain magnetic field strength, the fiber is placed at a distance from the pole of the permanent magnet, where the certain magnetic field strength can be achieved. The experiment was done under a stereo microscope (Zeiss Germany) coupled with a CCD camera as shown in figure 4-4 (a) and 4-4 (b). The bending deformation was observed for field strengths 167.242 mT, 154.993 mT, 143.679 mT, 133.745 mT and 124.832 mT achieved by putting the fiber from the pole of the magnet at the distance of 5 mm, 5.5 mm, 6 mm, 6.5 mm and 7 mm respectively. A piece of white paper was used as a scale to mark the distances between the magnet pole and the fiber to immediately get the value of the magnetic field strength that the fiber would experience at that distance. At first the ferrogel fiber was put on the stage of the microscope and the permanent magnet was then put at the specified distance to get the required field strength. As soon as the magnet was put in front of the ferrogel fiber, bending of the fiber was observed through the microscope. Digital image processing software Axivision 4.7 was used to capture the video of the bending deformation experiment. The time lapse module of the software was used to capture the video. The value of the maximum deformation of the fiber was measured by post processing the images that was captured form the video of the time-lapse module of the digital image processing software. Using the scaling option of the axiovision software, the deformation of the fiber can be measured. An example of measuring the deformation of a fiber of 4000 μm length and 1% volume ratio of magnetic particle using the axiovision software is shown in figure 4-5.

4.2.2 Results and Discussions

The bending deformation of ferrogel fibers were determined experimentally by changing the aspect ratio of the fiber, varying the volume ratio of the ferrofluid content of the ferrogel fibers and by varying the magnetic field strength (for each aspect ratio and volume fraction). The results obtained were then compared with those obtained from the finite element simulation of the micro-ferrogel fibers presented in chapter 3 of this thesis.

Figure 4-6 shows the maximum deformation vs. volume fraction of magnetic particle, obtained from simulation and experiments of the ferrogel fibers. It is found that, there is significant deviation between the experimental and simulation results. But the nature of the variation of the maximum deformation with the volume fraction of magnetic particle is very similar in both cases. The deviation between the experimental and simulation results are may be due to the idealizations that were made during the simulations, for example

1. In simulation it was assumed that the ferrogel structure is a homogenous mixture of 2-HEMA hydrogel precursor and ferrofluid, but during fabrication it was not easy to make a homogeneous mixture of ferrofluid and precursor, because the ferrofluid has a tendency to clump together.

2. The young's modulus of the ferrogel fiber depends on the fabrication parameters, like UV intensity, UV time exposure etc. The UV intensity was measured during the experiment and using that intensity and time exposure Young's modulus was found 450000 kpa from the lab calibration chart of young's modulus of 2-HEMA hydrogel. As a small tolerance exists between the photomask and the hydrogel precursor; it is not easy to measure the intensity of the UV light intensity that will reach the precursor. As a result, the young's modulus that was used in

the simulation from the calibration chart is exactly not the same as the experimental condition. This may cause a little variation in the deformation values.

Figure 4-7 shows the maximum deformations of the ferrogel fibers as a function of the magnetic field strength for fibers of AR 40 and 1% volume ratio. Both the experimental and numerical results are plotted on the same graph. It is seen from the figure that, the nature of variation of the deformation with the field strength is similar in both the cases, but there is a deviation between the two results. The probable reasons of the deviations are described above.

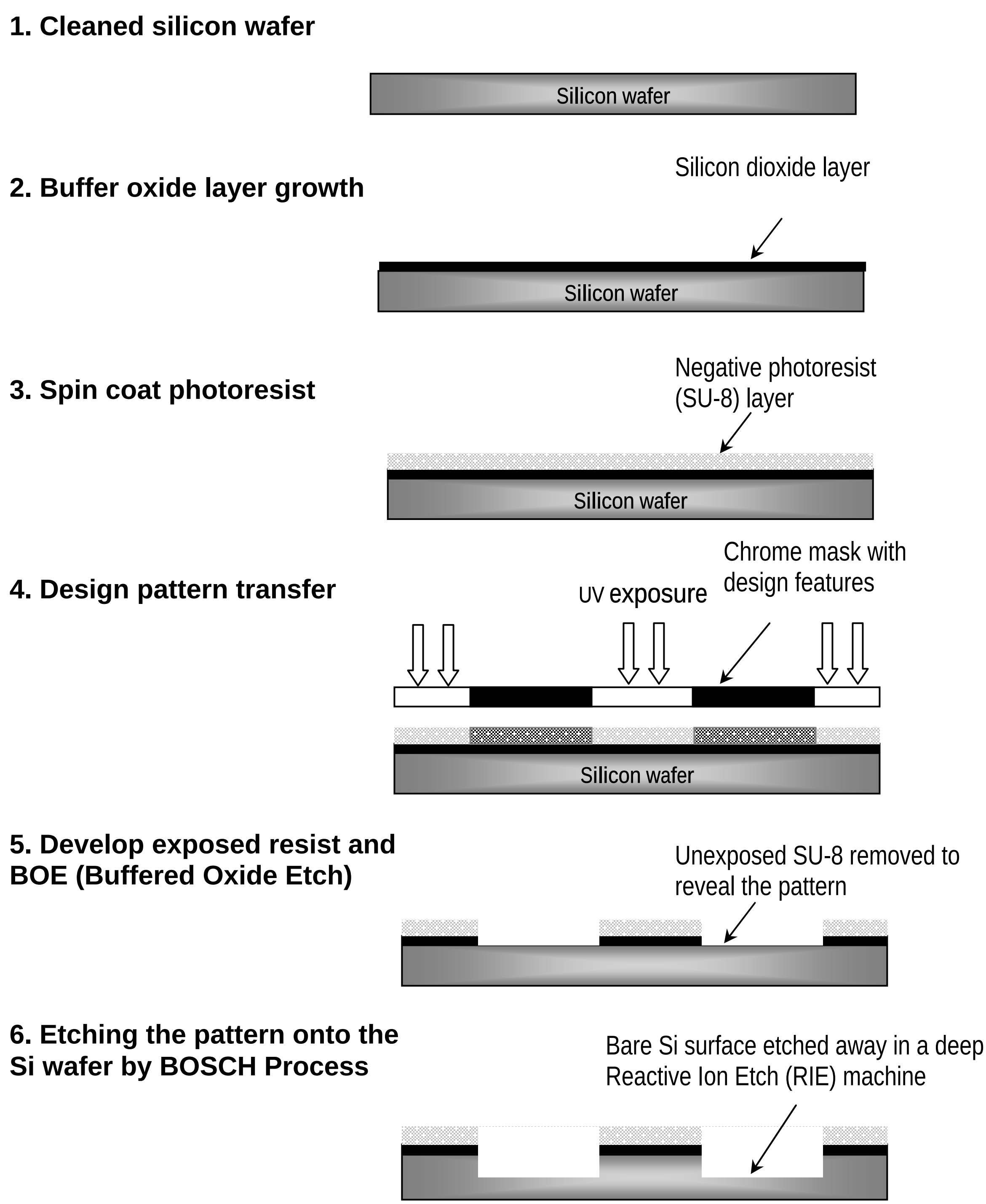

Figure 4-1: Steps of fabricating silicon master

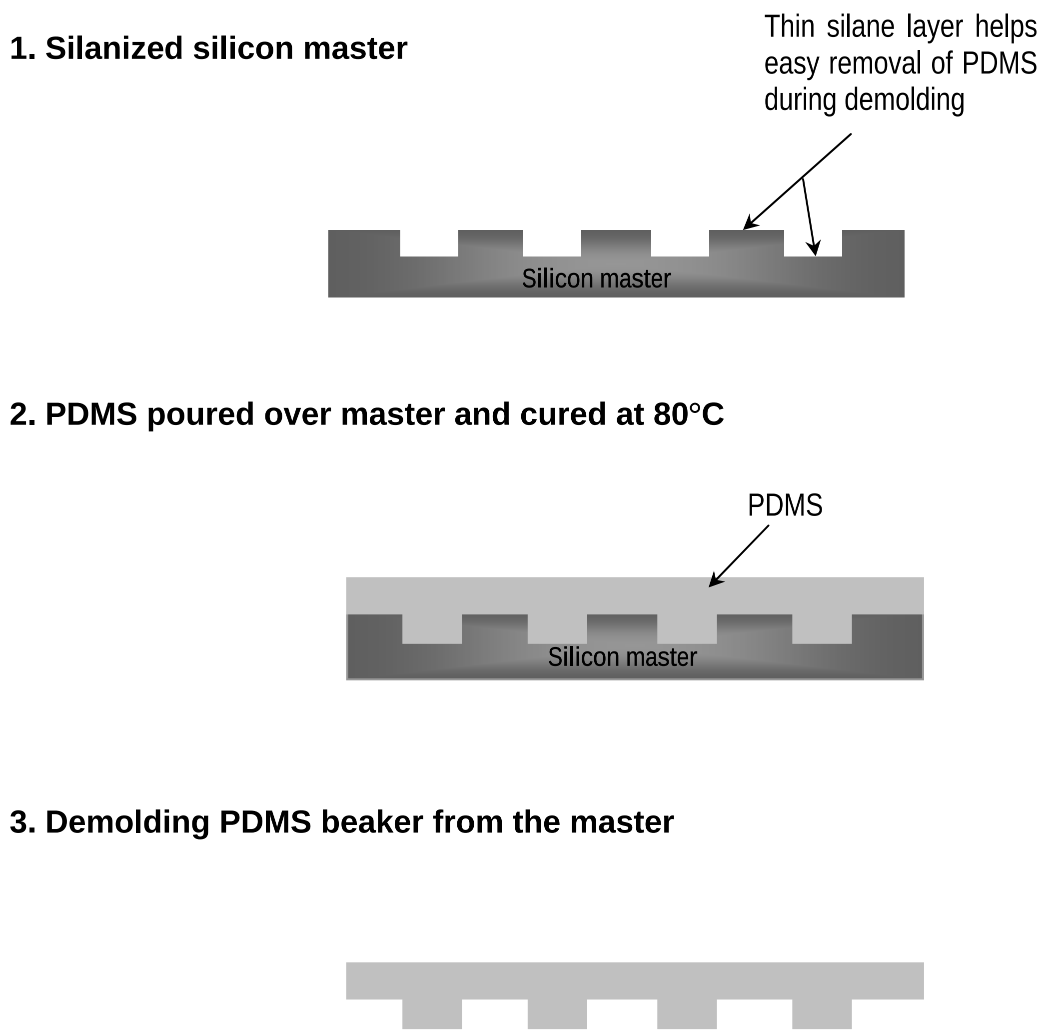

Figure 4-2: Steps of fabricating PDMS micro-beakers

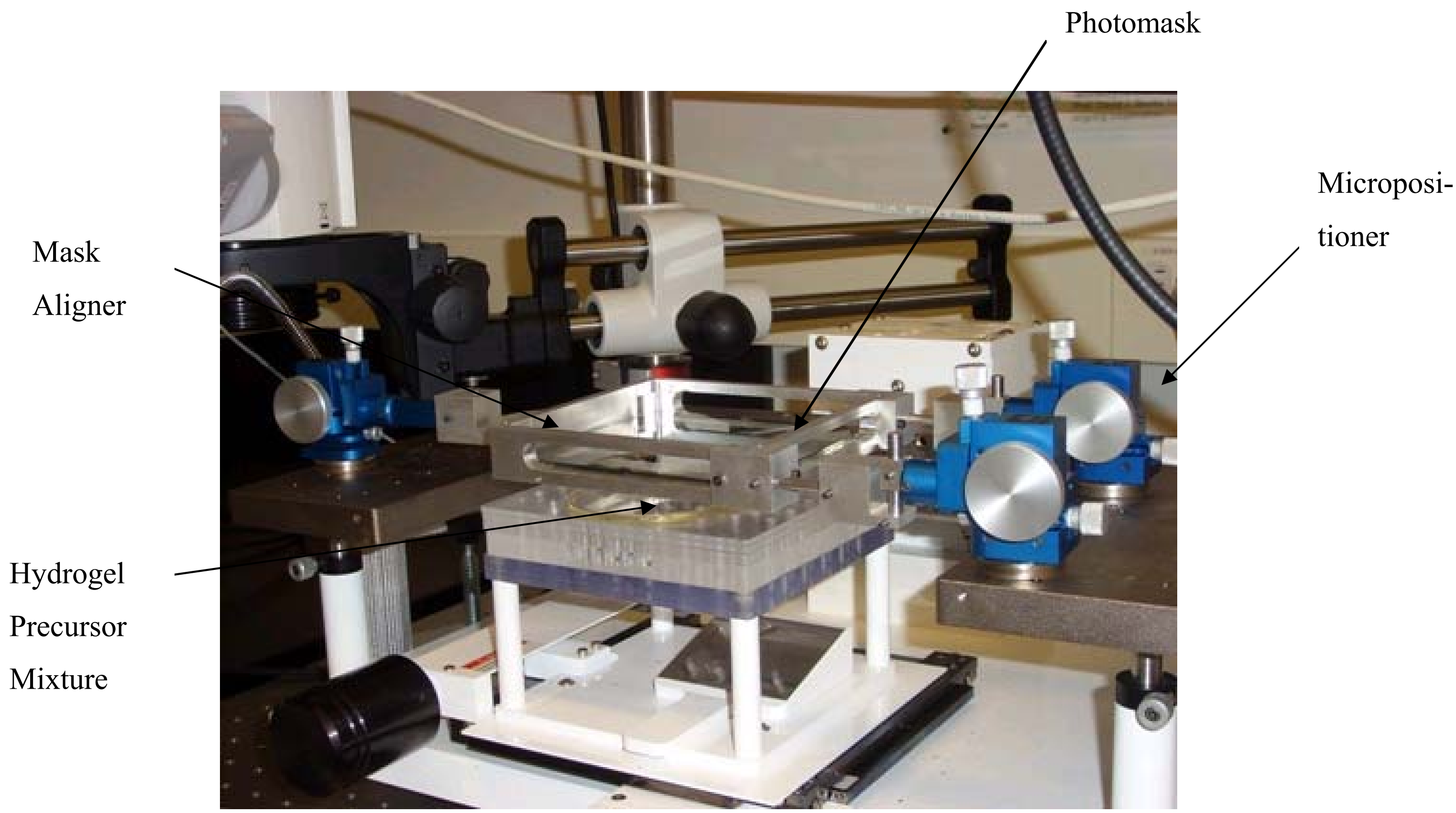

Figure 4-3: The arrangement of the mask-aligner and the photomask used to polymerize the ferrogel precursor

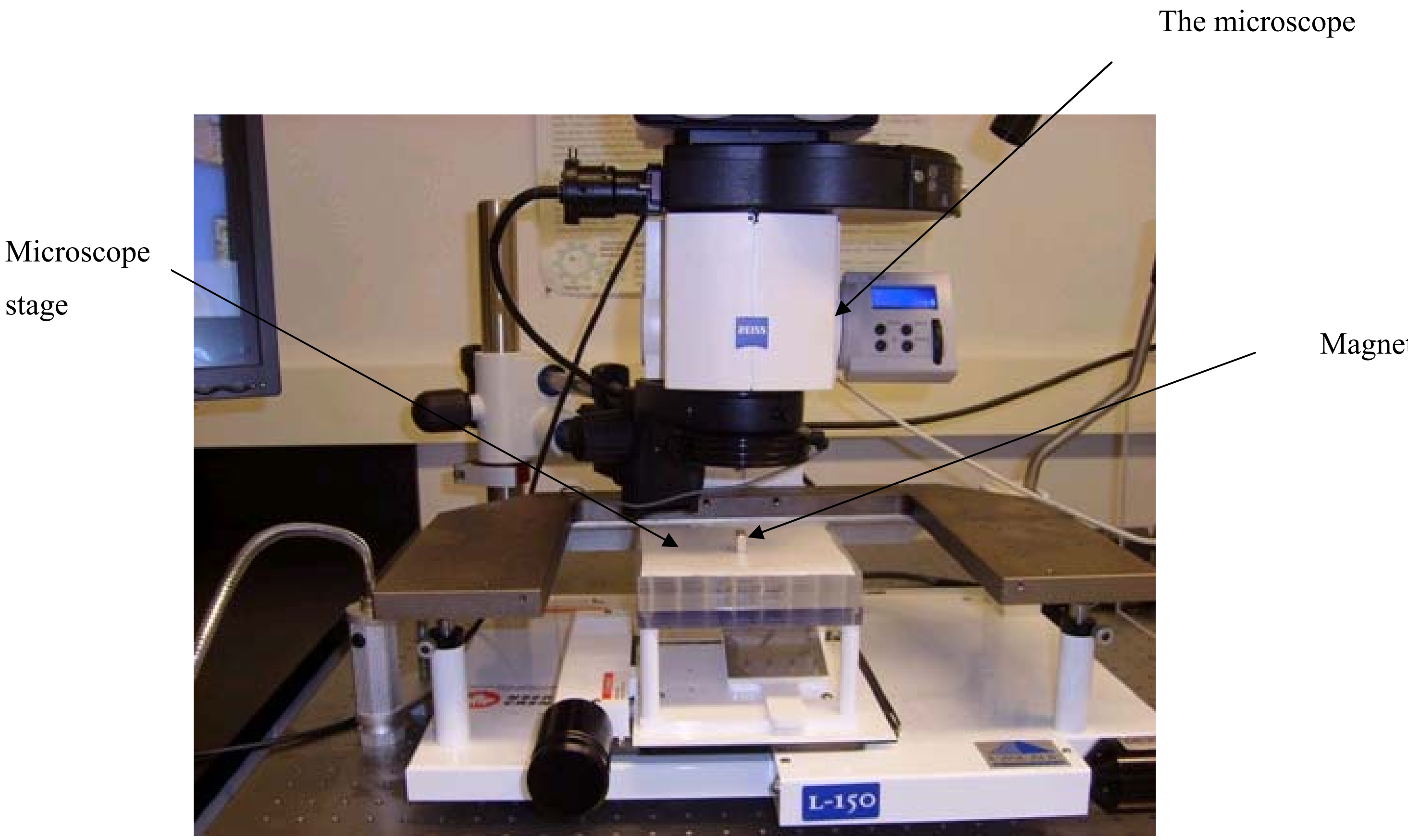

Figure 4.4 (a): The Experimental Setup

Figure 4-4 (b): The microscope equipped with the camera

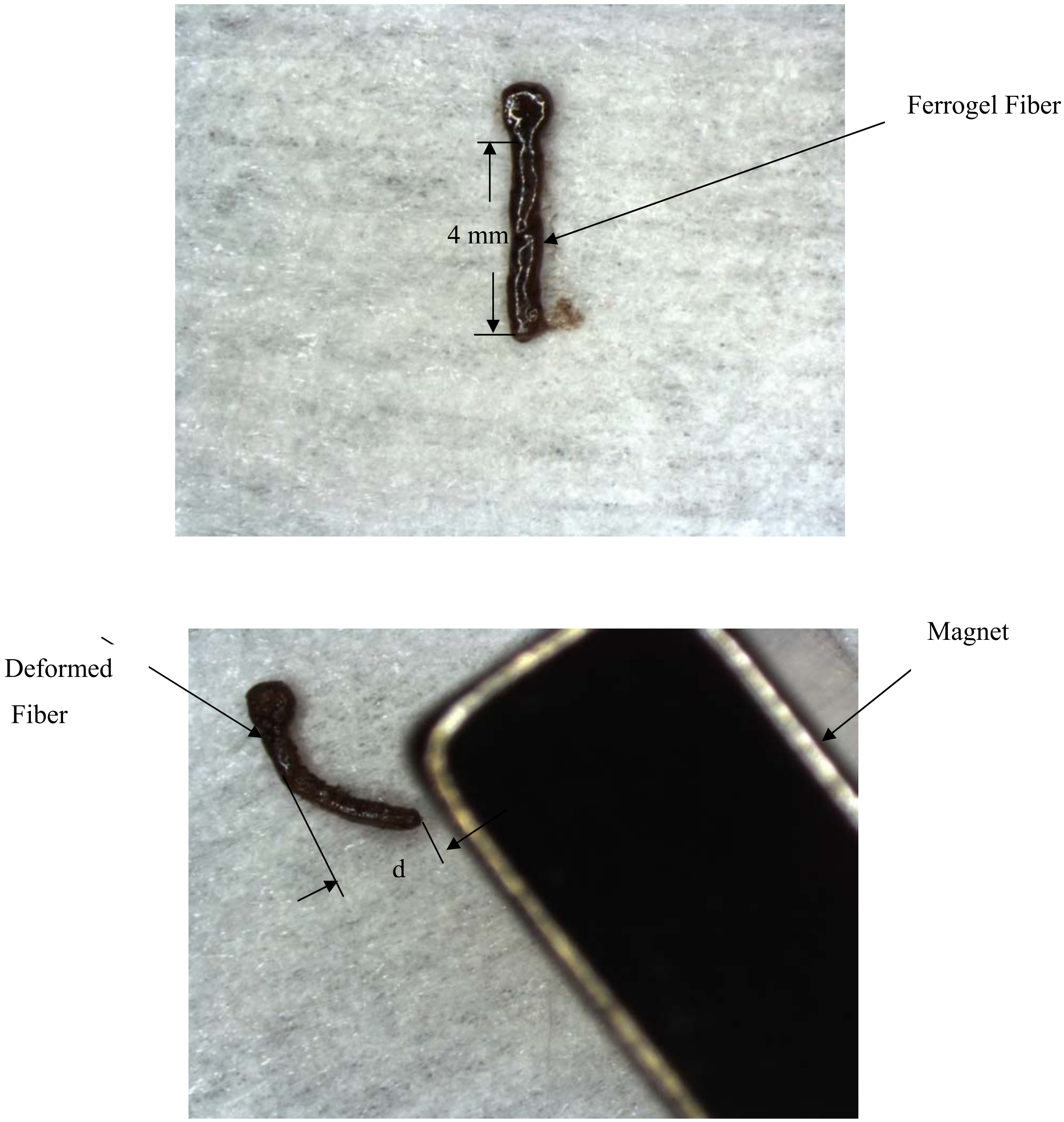

Figure 4-5: The method of measuring the bending deformation of the ferrogel fiber

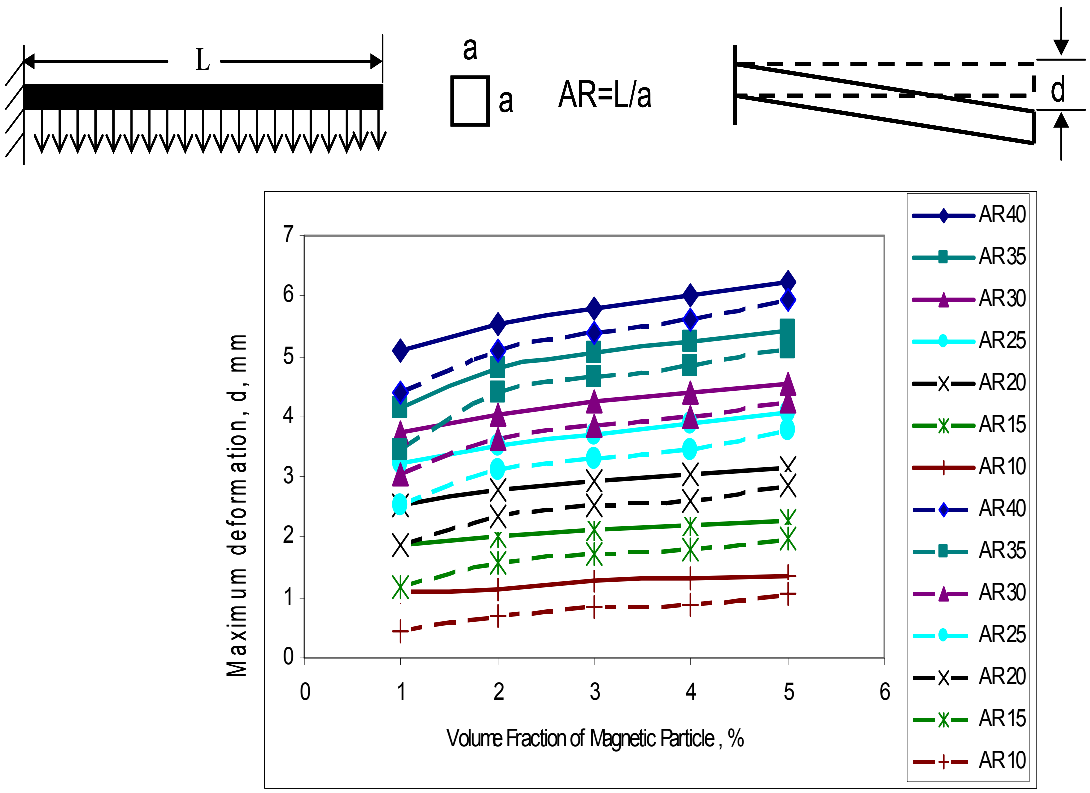

Figure 4-6: Comparison between Experimental and Simulation deformation of the ferrogel fibers. The dotted lines indicate numerical results and the solid lines indicate experimental results

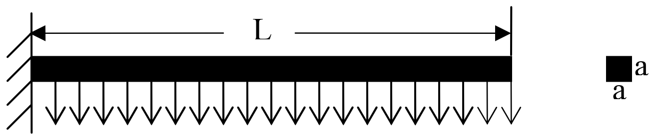

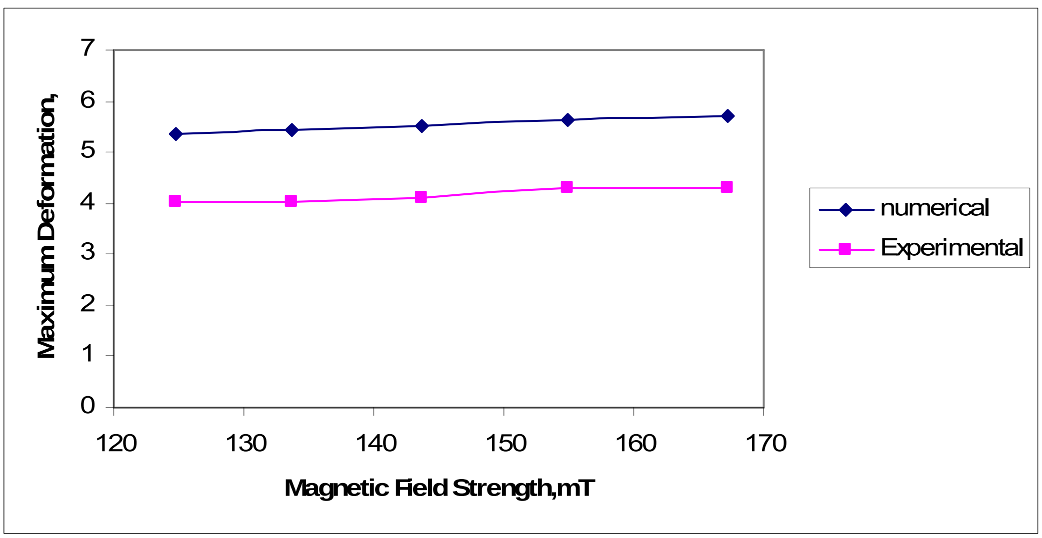

Figure 4-7: Comparison between numerical and experimental results for the maximum deformation due to the variation of magnetic field strength (AR 40, 1% VR)

CHAPTER 5

CONCLUSION AND FUTURE WORK

A micro ferrogel fiber was developed and deformed in bending using a non-uniform magnetic field. It is found that the maximum deformation of ferrogel fiber increases non-linearly with the increase of the volume fraction of magnetic particle embedded in the fiber.The increase of the aspect ratio of the ferrogel fiber was also found to increase the maximum deformation non-linearly at its free tip. For a fixed aspect ratio and volume fraction, the maximum deformation increases linearly with increase in the magnetic field strength.

Developed the fabrication process of micro ferrogel fibers. Numerical investigation of actuation of both straight and stepped ferrogel fibers in a non-uniform magnetic filed is performed. Experimental study of actuation of micro-ferrogel fibers is performed in a non-uniform magnetic field.

A process for the prototyping of a stepped fiber should be developed and experimental testing and comparison with numerical result should be performed. Deformation of different shapes of fibers can be investigated experimentally and numerically to find a better way to bend a free ferrogel fiber .A novel method for bending the fiber in a free-free configuration should be developed.

BIBLIOGRAPHY

1. Peppas, N.A., Bures, P., Leobandung, W., and Ichikawa, H.,European Journal of Pharmaceutics and Biopharmaceutics, 2000. **50**(1): p. 27-46.
2. Liu, R.H., Yu, Q., and Beebe, D.J.,Journal of Microelectromechanical Systems, 2002. **11**(1): p. 45-53.
3. Malmonge, S.M., Zavaglia, C.A.C., and Belangero, W.D.,Brazilian Journal of Medical and Biological Research, 2000. **33**(3): p. 307-312.
4. Herber, S., Olthuis, W., and Bergveld, P.,Sensors and Actuators B-Chemical, 2003. **91**(1-3): p. 378-382.
5. Beebe, D.J., Moore, J.S., Bauer, J.M., Yu, Q., Liu, R.H., Devadoss, C., and Jo, B.H.,Nature, 2000. **404**(6778): p. 588-590.
6. Zrinyi, M., Barsi, L., and Buki, A.,Journal of Chemical Physics, 1996. **104**(21): p. 8750-8756.
7. Zrinyi, M., Barsi, L., and Buki, A.,Polymer Gels and Networks, 1997. **5**(5): p. 415-427.
8. Zrinyi, M., Barsi, L., Szabo, D., and Kilian, H.G.,Journal of Chemical Physics, 1997. **106**(13): p. 5685-5692.
9. Zrinyi, M.,Trends in Polymer Science, 1997. **5**(9): p. 280-285.
10. Zrinyi, M., Szabo, D., and Barsi, L.,Journal of Intelligent Material Systems and Structures, 1998. **9**(8): p. 667-671.
11. Zrinyi, M., Szabo, D., and Kilian, H.G.,Polymer Gels and Networks, 1998. **6**(6): p. 441-454.
12. Zrinyi, M.,Colloid and Polymer Science, 2000. **278**(2): p. 98-103.

13. Zrinyi, M. and Szabo, D.,International Journal of Modern Physics B, 2001. **15**(6-7): p. 557-563.

14. Ramanujan, R.V. and Lao, L.L.,Smart Materials & Structures, 2006. **15**(4): p. 952-956.

15. M.Hillery, A., W.Lloyd, A., and Swarbrick, J., *Drug Delivery and Targeting for Pharmacists and Pharmaceutical Scientists*. 1 ed. 2001, London: Taylor and Francis.

16. El-Nokaly, M.A., M.Piatt, D., and Charpeniter, B.A., *Polymeric Delivery Systems - Properties and Applications*. 1st ed. 1992, San Francisco: Library of Congress cataloging-in-Publication Data.

17. Torchilin, V.P.,European Journal of Pharmaceutical Sciences, 2000. **11**: p. S81-S91.

18. Vogelson, C.T.,Modern Drug Delivery, 2001. **4**(4): p. 49-50,52.

19. Henry, C.M., *Drug Delivery*, in *The Newsmagazine of the Chemical World*. 2002. p. 39-47.

20. Masteikova, R., Chalupova, Z., and Sklubalova, Z.,Medicina (Kaunas), 2003. **39**(Suppl. 2): p. 19-24.

21. Qui, Y. and Park, K.,Advanced Drug Delivery, 2001. **53**: p. pp. 321-339.

22. De, S.K., Aluru, N.R., Johnson, B., Crone, W.C., Beebe, D.J., and Moore, J.,Journal of Microelectromechanical Systems, 2002. **11**(5): p. 544-555.

23. Aluru, A.N.C.Q.Y.J.S.M.a.N.R.,Journal of Aerospace Engineering, 2003: p. 55-64.

24. Aribe,proc. of SPIE, 2006. **6343**: p. 1-9.

25. Zhang, Y.L., Won, C.Y., and Chu, C.C.,Journal of Polymer Science Part a-Polymer Chemistry, 1999. **37**(24): p. 4554-4569.

26. Chu, Y., Varanasi, P.P., Mcglade, M.J., and Varanasi, S.,Journal of Applied Polymer Science, 1995. **58**(12): p. 2161-2176.

27. Hoffman, A.S.,Bioartificial Organs Iii: Tissue Sourcing, Immunoisolation, and Clinical Trials, 2001. **944**: p. 62-73.

28. Wallmersperger, T., Kroplin, B., and Gulch, R.W.,Mechanics of Materials, 2004. **36**(5-6): p. 411-420.

29. Satish,Indian Journal of Pharmaceutical Sciences, 2006. **68**(2): p. 133-140.

30. Jabbari, E. and Nozari, S.,European Polymer Journal, 2000. **36**(12): p. 2685-2692.

31. Beebe, D.J., Moore, J.S., Bauer, J.M., Yu, Q., Liu, R.H., Devadoss, C., and Jo, B.H.,Nature, 2000. **404**(6778): p. 588-+.

32. Jabbari, E. and Nozari, S.,Iranian Polymer Journal, 1999. **8**(4): p. 263-270.

33. Park, J.Y., Oh, H.J., Kim, D.J., Baek, J.Y., and Lee, S.H.,Journal of Micromechanics and Microengineering, 2006. **16**(3): p. 656-663.

34. Kim, D., Kim, S., Park, J., Baek, J., Kim, S., Sun, K., Lee, T., and Lee, S.,Sensors and Actuators a-Physical, 2007. **134**(2): p. 321-328.

35. Jin, X. and Hsieh, Y.L.,Macromolecular Chemistry and Physics, 2005. **206**(17): p. 1745-1751.

36. Sahoo, A., Ramasubramani, K.R.T., Jassal, M., and Agrawal, A.K.,European Polymer Journal, 2007. **43**(3): p. 1065-1076.

37. van der Linden, H., Olthuis, W., and Bergveld, P.,Lab on a Chip, 2004. **4**(6): p. 619-624.
38. Gottlieb, R., Schmidt, T., and Arndt, K.F.,Nuclear Instruments & Methods in Physics Research Section B-Beam Interactions with Materials and Atoms, 2005. **236**: p. 371-376.
39. Caykara, T., Kiper, S., and Demirel, G.,European Polymer Journal, 2006. **42**(2): p. 348-355.
40. Caykara, T., Kucuktepe, S., and Turan, E.,Macromolecular Materials and Engineering, 2006. **291**(10): p. 1278-1286.
41. Caykara, T., Sila, K., and Turan, E.,Polymer International, 2007. **56**(4): p. 532-537.
42. Zhao, Q., Sun, J.Z., and Zhou, Q.Y.,Journal of Applied Polymer Science, 2007. **104**(6): p. 4080-4087.
43. Zhang, J. and Peppas, N.A.,Macromolecules, 2000. **33**(1): p. 102-107.
44. Xue, W., Champ, S., and Huglin, M.B.,Polymer, 2001. **42**(8): p. 3665-3669.
45. Didukh, A.G., Koizhaiganova, R.B., Khamitzhanova, G., Bimendina, L.A., and Kudaibergenov, S.E.,Polymer International, 2003. **52**(6): p. 883-891.
46. Sun, S. and Mak, A.F.T.,Journal of Polymer Science Part B-Polymer Physics, 2001. **39**(2): p. 236-246.

47. Al-Aribe, K., Knopf, G.K., and Bassi, A.S. *Photo-responsive hydrogel for controlling flow on a microfluidic chip*. in *Photonics North 2006*. 2006: SPIE.

48. Zourob, M., Ong, K.G., Zeng, K.F., Mouffouk, F., and Grimes, C.A.,Analyst, 2007. **132**(4): p. 338-343.

49. Lei,2004.

50. Kim, S.J., Park, S.J., and Kim, S.I.,Smart Materials & Structures, 2004. **13**(2): p. 317-322.

51. De, S.K. and Aluru, N.R.,Mechanics of Materials, 2004. **36**(5-6): p. 395-410.

52. Kim, B., La Flamme, K., and Peppas, N.A.,Journal of Applied Polymer Science, 2003. **89**(6): p. 1606-1613.

53. Bassetti, M.J., Chatterjee, A.N., Aluru, N.R., and Beebe, D.J.,Journal of Microelectromechanical Systems, 2005. **14**(5): p. 1198-1207.

54. Shiga, T. and Kurauchi, T.,Journal of Applied Polymer Science, 1990. **39**(11-12): p. 2305-2320.

55. Osada, Y., Gong, J.P., and Tanaka, Y.,Journal of Macromolecular Science-Polymer Reviews, 2004. **C44**(1): p. 87-112.

56. Kim, S.J., Kim, H.I., Park, S.J., Kim, I.Y., Lee, S.H., Lee, T.S., and Kim, S.I.,Smart Materials & Structures, 2005. **14**(4): p. 511-514.

57. Li, H., Wang, X.G., Wang, Z.J., and Lam, K.Y.,Macromolecular Bioscience, 2005. **5**(9): p. 904-914.

58. Qui Y, P.K.,Advancrd Drug Delivery, 2001. **53**: p. 321-339.

59. Xue, W., Hamley, I.W., and Huglin, M.B.,Polymer, 2002. **43**(19): p. 5181-5186.

60. Ozturk, V. and Okay, O.,Polymer, 2002. **43**(18): p. 5017-5026.

61. Yin, L., Yuan, Z., and He, L.H.,Computational Materials Science, 2004. **31**(3-4): p. 299-308.

62. Aribe. *Photo-Responsive Hydrogel for controlling flow on a microfluidic chip*. in *proc. of SPIE*. 2006.

63. Mamada,Macromolecules, 1989. **23**(5): p. 1517-1519.

64. Suzuki, A. and Tanaka, T.,Nature, 1990. **346**(6282): p. 345-347.

65. Suzuki, A., Ishii, T., and Maruyama, Y.,Journal of Applied Physics, 1996. **80**(1): p. 131-136.

66. Shang, *Fiber Deformation in AC Magnetic Field*, in *Department of Mechanical Engineering*. 2004, University of Alberta: Edmonton. p. 76.

67. Szabo, D. and Zrinyi, M.,International Journal of Modern Physics B, 2002. **16**(17-18): p. 2616-2621.

68. Chatterjee, J., Haik, Y., and Chen, C.J.,Colloid and Polymer Science, 2003. **281**(9): p. 892-896.

69. Lao, L.L. and Ramanujan, R.V.,Journal of Materials Science-Materials in Medicine, 2004. **15**(10): p. 1061-1064.

70. Barsi, L., Szabo, D., Buki, A., and Zrinyi, M.,Magyar Kemiai Folyoirat, 1997. **103**(9): p. 401-410.

71. Barsi, L. and Zrinyi, M.,Ach-Models in Chemistry, 1998. **135**(3): p. 241-246.

72. Zrinyi, M., Szilagyi, A., Filipcsei, G., Feher, J., Szalma, J., and Moczar, G.,Polymers for Advanced Technologies, 2001. **12**(9): p. 501-505.

73. Szabo, D., Barsi, L., Buki, A., and Zrinyi, M.,Ach-Models in Chemistry, 1997. **134**(2-3): p. 155-167.

74. Szabo, D., Szeghy, G., and Zrinyi, M.,Macromolecules, 1998. **31**(19): p. 6541-6548.

75. Barsi, L.,Progr Colloid Polym Sci, 1996. 102: p. 57-63.

76. Teixeira, A.V. and Licinio, P.,Journal of Magnetism and Magnetic Materials, 2005. 289: p. 126-128.

77. Scherer, C. and Neto, A.M.F.,Brazilian Journal of Physics, 2005. 35(3A): p. 718-727.

78. Rosensweig, Ferrohydrodynamics. 1st ed. 1985: Press Syndicate of the University of Cambridge. 339.

79. Zefeng X, G.W., Kaixiong T, Jianxing L,journal of Huazhong University of Science and Technology-Medical Sciences, 2005. 25(1): p. 59-61.

80. Saunders J.R, A.-S.S., Khaleque.T, Hanula .S, Moussa. W,Journal of Computational and Theoritical Nanoscience, 2008. 5: p. 1-19.

81. Donea, J., A. Huerta, J.-P. Ponthot, A. Rodriguez-Ferran, Arbitrary Langrangian Eulerian Methods. Encyclopedia of computational Mechanics. 2004: Fundamentals John Wiley and Sons ltd.

APPENDIX A

A.1 Magnetic Dipoles

Magnetic Dipole Moment is a vector pointing out of the plane of the current loop. It has the magnitude equal to the product of the current and loop area. The area vector, and the direction of the magnetic dipole moment, is given by a right-hand rule using the direction of the currents.

$$\vec{\mu} \equiv i\vec{A}$$

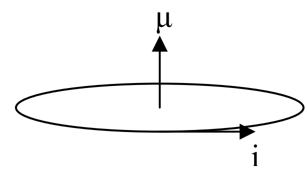

A.2 Magnetic Dipole Interaction in External Fields

Torque :

By the **F**=*i***L×B**$_{ext}$ force law, we know that a current loop (and thus a magnetic dipole) feels a torque when placed in an external magnetic field:

$$\boldsymbol{\tau} = \boldsymbol{\mu} \times \mathbf{B}_{ext}$$

The direction of the torque is to line up the dipole moment with the magnetic field

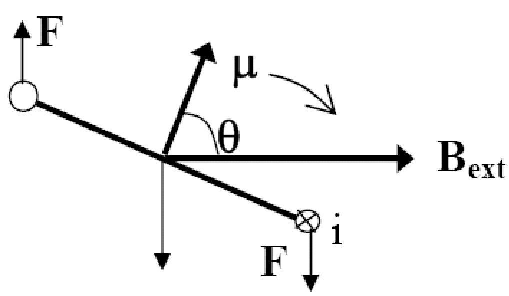

Potential Energy:

Since the magnetic dipole wants to line up with the magnetic field, it must have higher potential energy when it is aligned opposite to the magnetic field direction and lower potential energy when it is aligned with the field. The work done by the magnetic field when aligning the dipole is calculated.

θ is the angle between the magnetic dipole direction and the external field direction. The potential energy of the dipole is the negative of the work done by the field:

$U = -W = \int \tau d\theta$

The zero-point of the potential energy is arbitrary, so it's taken to be zero when θ=90°.

Then,

$$U = +\int_{\frac{\pi}{2}}^{\theta} \tau d\theta = \int_{\frac{\pi}{2}}^{\theta} \mu B \sin\theta' d\theta'$$

The positive sign arises because $\tau . d\theta = -\tau d\theta$, τ and θ are oppositely aligned. Thus

$$U = -\mu . B$$

The lowest energy configuration is for μ and B parallel. Work is required to re-align the magnetic dipole in an external B field.

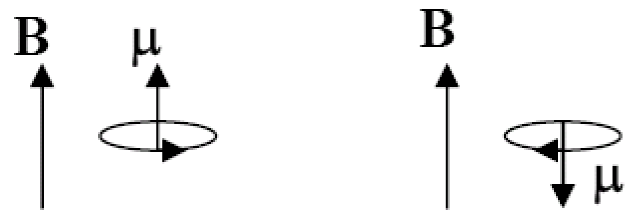

Lowest Energy Highest energy

The change in energy required to flip a dipole from one alignment to the other is

$$\Delta U = 2\mu B$$

A.3 Force on a Magnetic Dipole in a Non-uniform Filed

Two bar magnets stick together when opposite poles are brought together (north-south), and repel when the same poles are brought together (north-north, south-south). The magnetic field of a small bar magnet is equivalent to a small current loop, so two magnets stacked end-to-end vertically are equivalent to two current loops stacked

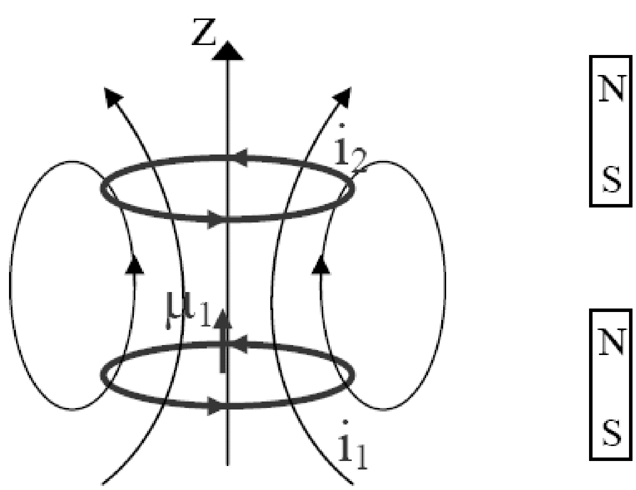

The potential energy on one dipole from the magnetic field from the other is:

$$U = -\mu_1.B_2 = -\mu_{z1}B_{z2}$$

Now force is derived from the rate of change of the potential energy

$$F = -\nabla U = -\frac{\partial U}{\partial z}\hat{z}$$

For example, the gravitational potential energy of a mass a distance z above the surface of the Earth can be expressed by U= mgz. Thus, the force is F = -mgz (i.e. down)

For the case of the stacked dipoles

$$F_z = -\frac{\partial U}{\partial z} = \mu_{1z}\frac{\partial B_{2z}}{\partial z}$$

or in general, any magnetic dipole placed in a non-uniform B-field

$$F_z = \mu_z \frac{\partial B}{\partial z}$$

Thus there is force acting on a dipole when placed in a non-uniform magnetic field.

APPENDIX B

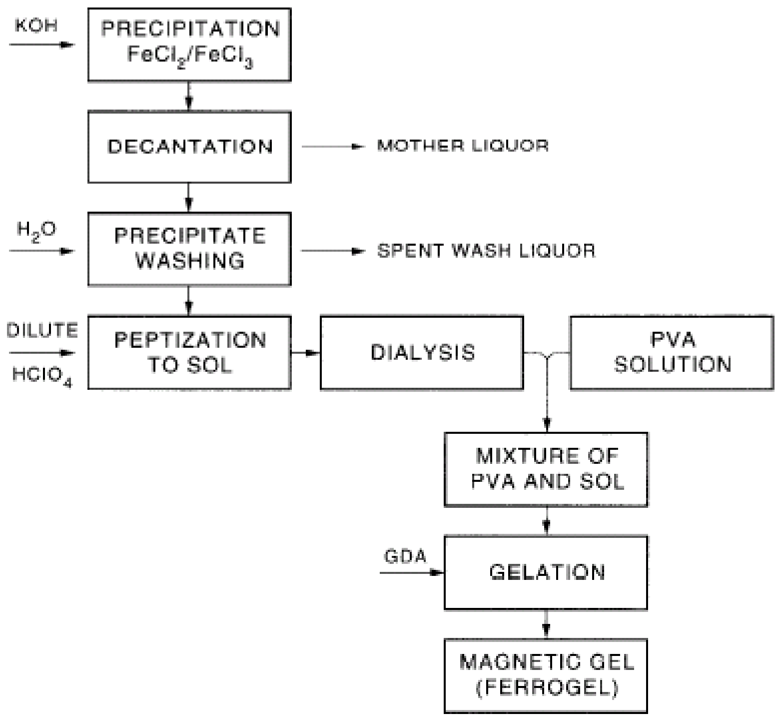

KOH
PRECIPITATION
FeCl2/FeCl3
DECANTATION
MOTHER LIQUOR
H2O
PRECIPITATE
WASHING
SPENT WASH LIQUOR
DILUTE
HClO4
PEPTIZATION
TO SOL
DIALYSIS
PVA
SOLUTION
MIXTURE OF
PVA AND SOL
GDA
GELATION
MAGNETIC GEL
(FERROGEL)